Volume II
Appendix D.16

Determination of Debris Risk to the Public Due to the *Columbia* Breakup During Reentry

List of Figures

List Of Tables

THIS PAGE INTENTIONALLY LEFT BLANK

Determination of Debris Risk to the Public Due to the *Columbia* Breakup During Reentry

Technical Report No. 03-517-01
Prepared for the Columbia Accident Investigation Board
Under Subcontract to Valador, by Mark Y. Y. Lin, Erik W. F. Larson, and Jon D. Collins: ACTA Inc.
September 2003

ACKNOWLEDGEMENTS

This work was performed under subcontract to Valador, Inc. for the Columbia Accident Investigation Board. The work was awarded as the result of a competitive procurement. Dr. Daniel Heimerdinger monitored and was administrator for the contract.

The project manager for the work by ACTA was Dr. Jon D. Collins. Dr. Mark Lin developed the debris model and performed the ground risk analysis. Dr. Erik Larson developed the population model and performed the aircraft risk analysis. In addition, Dr. Keng Yap performed the simplified casualty area computations, Bud Parks provided the meteorological data and Dr. Steven Carbon modified the CRTF program to be able to compute P(≥ 1 casualties).

ACTA acknowledges Dr. Paul Wilde of the Federal Aviation Administration and Elizabeth Fountain of the Columbia Task Force in furnishing the field data used in this study. Dr. Wilde also monitored the progress of the work and provided very helpful direction.

SUMMARY

This report provides the findings from a study initiated by the Columbia Accident Investigation Board to determine if the lack of casualties from the large number of Columbia fragments would have been the expected. The study was based upon the last reported position of the vehicle, the impact locations (latitude and longitude) of all of the recovered debris, the total weight (sum) of the recovered debris and some data (material, two dimensions) on some of the pieces of debris. The study was performed before any more detailed evaluation of the debris was available. The process used in the study involved the following steps:

1. Create a mathematical model of the Columbia (STS-107) breakup debris in terms of size, weights, numbers, aerodynamic characteristics and origins (initial time, position). This model is based on the best available information at the time the study was started, which was in late May of 2003. Ground search activity for the debris recovery effort continued at full strength until April 25, and then gradually tapered off as the search was completed. Therefore, the data needed for this study was not available until late May.
2. Develop a "population library" that describes where people were most likely to be located and whether and how they were sheltered. The population study assumed that about 18% of the people were probably outdoors and the remaining in various levels of sheltering.
3. Simulate the debris cloud and develop probabilistic impact dispersions for the debris impacts. The paths of the fall of the debris fragments take into consideration the best estimate of the wind conditions (measured in terms of speed and direction and as a function of altitude) at the time of the event. Wind data was available from the Dallas Fort Worth Airport and the airport at Shreveport, Louisiana.
4. Determine the expected number of casualties, E_C, considering the debris impact distributions, estimated locations of people, sheltering of people and the vulnerability of people to inert debris impacts.
5. Estimate the probability of any impact to aircraft in the vicinity of the debris cloud.

The CRTF (Common Real-Time Debris Footprint) program operating inside the RRAT (Range Risk Analysis Tool) was used to perform the risk analysis. The results are summarized in the table at the top of the next page.

There is no certainty as to the amount of debris that survived. The range of possibilities is from the gathered debris being all of the debris that survived to all of the Columbia debris surviving, but not having been located. The table presents that range with the assumption that the mix of the gathered debris is representative of the mix at every other survival percentage. The column containing P(≥1 Casual-

Debris Case	*Percentage of Total Orbiter and Payload Weight*	*E_C (Including sheltering)*	*P(≥1 Cas.)[1] (Including sheltering)*
Model (gathered debris)	38%	0.14	0.13
60% of total wt. survived	60%	0.21	0.19
80% of total wt. survived	80%	0.29	0.25
100% of total wt. survived	100%	0.37	0.30

ties) provides an estimate of the probability of one or more casualties. It is a probability with range of $0 \leq P \leq 1$ whereas the E_C is an average that can have a value that exceeds 1.

Individual risk was also computed. The highest probability of any particular person exposed to the recovered debris becoming a casualty was determined to be 7.6×10^{-5}.

A preliminary study of the risk to aircraft indicated that the expected number of planes impacted by the Columbia breakup was approximately 3×10^{-2}. This is primarily due to possible impacts with general aviation (>80%). The numbers were based on estimates of the aircraft density for similar conditions to those in another study, but not on actual statistics at the time of the accident.

The general conclusion is that the lack of casualties was the expected consequence, but not overwhelmingly so. Sheltering played an important role as well as the lower density of population in the region where the debris was recovered in reducing the likelihood of injuries among the general public. This study should be revisited when the debris data are cataloged more completely to determine if the model assumptions and results shift due to the finer debris resolution.

1. Introduction

There were no reported casualties due to debris from the breakup of the Columbia. *The primary purpose of the analysis in this report is to confirm whether the lack of casualties is the expected consequence, or whether this happened to be good fortune for the people on the ground exposed to the debris*.

The Columbia Accident Investigation Board (CAIB) contracted with ACTA Inc. to accomplish this task using the debris data available at the time. The process used in the study involved the following steps:

1. Create a mathematical model of the Columbia (STS-107) breakup debris in terms of size, weights, numbers, aerodynamic characteristics and origins (initial time, position). This model is based on the best available information at the time the study was started.
2. Develop a "population library" that describes where people are located and whether and how they are sheltered. This is to take into consideration as to where people would most likely be at the time of the event.
3. Simulate the debris cloud and develop probabilistic impact dispersions for the debris impacts. The fall of the debris takes into consideration the best estimate of the wind conditions (measured in terms of speed and direction and as a function of altitude) at the time of the event.
4. Use casualty models for people in the open and in structures, based on computed vulnerabilities of people and specific structure types, combined with the locations and numbers of people and probability of impact, to determine the expected number of casualties.
5. Make an estimate of the risks to aircraft in the vicinity of the debris cloud.
6. Use an alternate simplified model to estimate the risk to provide some logical validity to the risks computed by the more elaborate model.
7. Evaluate the sensitivity of the results to model parameters.

ACTA used the CRTF (Common Real-Time Debris Footprint) program [1] operating inside the RRAT (Range Risk Analysis Tool) [2] to perform the risk analysis. The CRTF program, described briefly in Appendix A, was originally developed to support the range safety work at the Air Force Eastern and Western Ranges.

The risk posed to people on the ground from launch vehicle flight is typically quantified in terms of expected casualties, which is the mean value from a statistical analysis of the probability and consequence of all foreseen outcomes of flight [3, 4]. A casualty is generally defined as a serious injury or worse, including death. A typical risk estimate for accidental debris impacts during ascent of an expendable rocket is about 0.00002 expected casualties for all members of the public, including over flight of Africa. The typical total of 0.00002 expected casualties for an expendable rocket ascent predicts an average of two seriously injured individuals located on the ground after 100,000 launches. The expected casualties is equal to the probability of at least one casualty times one casualty, plus the probability of two casualties times two casualties, plus the probability of three casualties times three casualties, etc.

2. Derivation Of The Breakup Debris Model

2.1 Overall Procedure

The CAIB provided the coordinates of 75,440 pieces of gathered debris in an EXCEL spreadsheet. No individual weights were provided as that information had not yet been developed at the time of this study, only the total weight of the gathered pieces (84,900 lbs). The spreadsheet also contained some useful descriptive information, including material and some dimensions, for about 15,470 pieces of

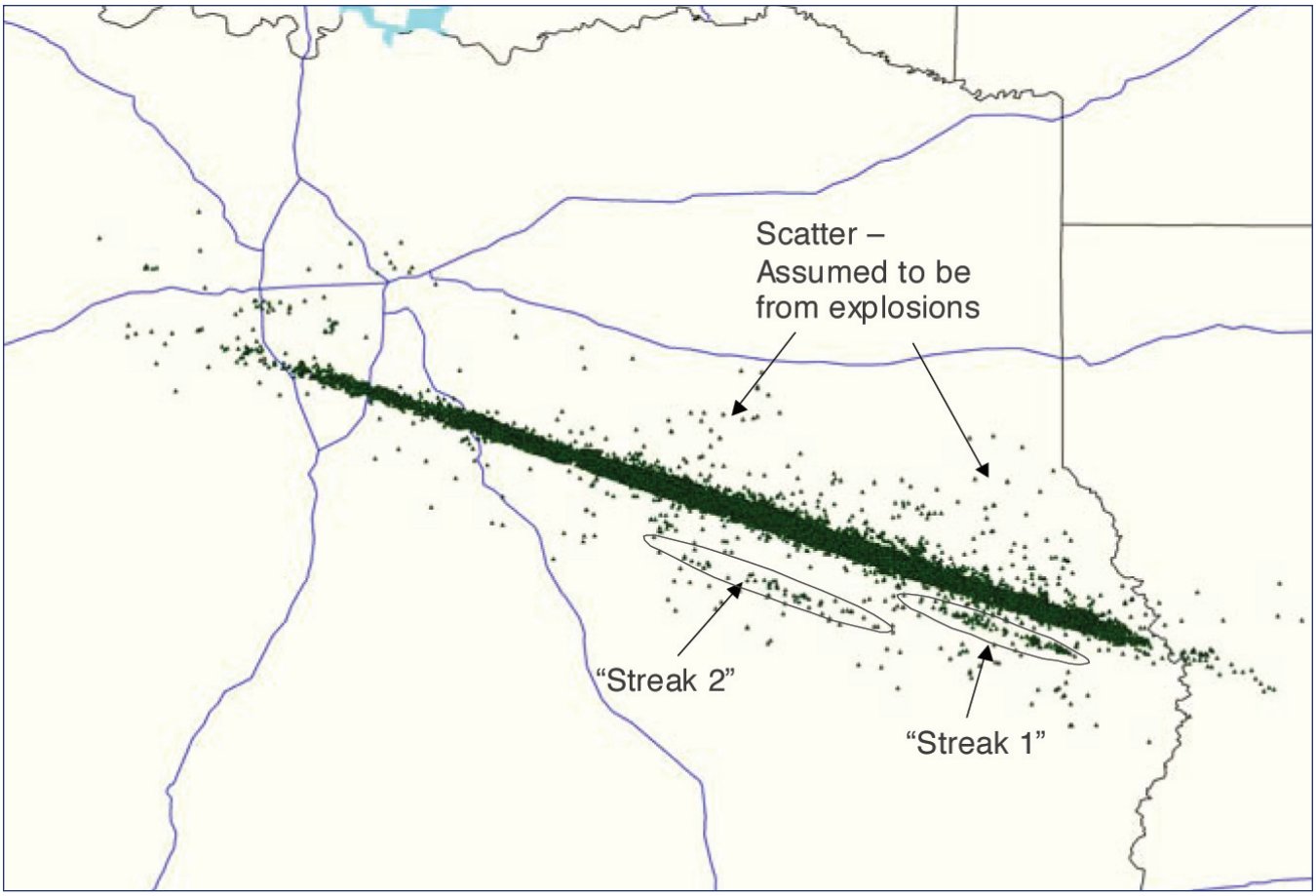

Figure 2-1. Locations of Recovered Debris.

debris. In addition, the CAIB provided the last state vector (position and velocity) communicated from the Columbia and a time-line of events.

The debris list developed for the study was extracted from the raw data in the EXCEL spreadsheet with a computer algorithm implemented to identify each fragment's composition, dimensions and shape. While errors were unavoidable in the processing of individual records, the overall weight of the constructed debris model and histogram of debris sizes and ballistic coefficients correlate well with observed data. It should be possible in later studies to remove more erroneous data by additional manual processing of the field records.

Figure 2-1 contains a map showing where the debris was recovered. A primary data grouping, Group 1, was used to account for the main debris field. Two secondary debris groups, Group 2 and Group 3 (identified as Streak 1 and Streak 2 in the figure) were created with separately fitted trajectories. Group 4 accounted for the widely scattered debris recovered outside of Group 1. The scatter observed in Group 4 debris seemed beyond the range that could be explained by lift, and thus it was assumed that a large velocity impulse of unknown source (an explosion?) was responsible. A standard deviation of 333 ft/sec in the velocity impulse produced a scatter that proved to be the best fit to the gathered Group 4 debris. There is no current explanation for the high velocities in Group 4, but the velocity impulse assumption enables the mathematical model to match the observed scatter. It will be shown later that the risks contributed by Groups 2, 3 and 4 are very small compared to Group 1 because of the relatively small numbers of pieces of debris in these groups. Therefore they do not contribute materially to the final result, and no further effort was put forth to model and explain the phenomenon.

2.2 Mechanics of Debris Fall and Dispersion

Before proceeding further, it is worthwhile to discuss the basic physics of falling debris. A piece of debris has an initial state vector that is defined by a position and velocity vector (six total components). The initial state vector may be perturbed from by an explosion that imparts a velocity and a consequential adjustment to the velocity vector. There is no adjustment to the initial position because the velocity is added impulsively. The gravity and aerodynamic forces affect the fall of the debris. Figure 2-2 shows a free-body diagram of a piece of debris. The dominant parameter in the trajectory computation is the ballistic coefficient represented by the Greek letter β. The formula for ballistic coefficient is

$$\beta = \frac{W}{C_D A}$$

where W is the weight of the fragment, C_D is the drag coefficient and A is a characteristic area associated with the drag coefficient. In this study the units for are lb/ft^2. This formula represents the ratio between inertial effects (W) and drag effects (C_DA). Objects with low weight to drag ratio fall much more slowly than objects with a high weight to drag ratio, e.g. a feather vs. a bowling ball.

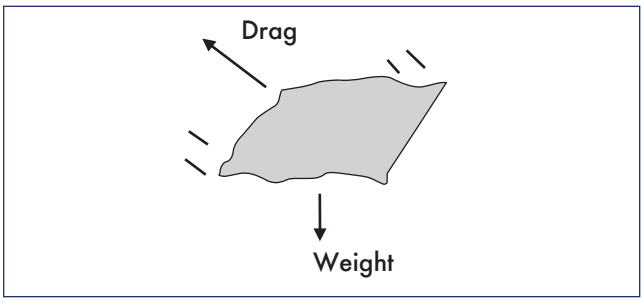

Figure 2-2. Free-Body Diagram of a Piece of Debris.

A fragment having an initial velocity with a horizontal component will travel further if it has a higher ballistic coefficient. As the debris falls it may come into equilibrium between the weight and the drag, resulting in falling at terminal velocity. At terminal velocity, and without the presence of wind, the fragment is falling vertically. At terminal velocity, the drag force, $1/2\ \rho V^2 C_D A$, equals the weight, W. This yields the equation,

$$V_{term} = \sqrt{\frac{2W}{\rho C_D A}} = \sqrt{\frac{2\beta}{\rho}}$$

which is equivalent to $V_{term} = 30\sqrt{\beta}$ at sea level, if β is expressed in lb/ft^2 and velocity in ft/s.

Wind is the other major factor affecting the fall of the debris. The effect, without explanation here, is proportional to $1/\sqrt{\beta}$. Thus, in summary, debris with smaller ballistic coefficients will fall closer to their initiation point, in the absence of winds, but will be moved more due to the wind (and in the direction of the wind). This is demonstrated in Figure 2-3.

The term Vacuum IP in the figure represents the impact point when there is no atmosphere, i.e. no drag. Note how the wind effect diminishes with increasing β.

2.3 Analysis of Gathered Debris

Data on 84,000 pieces of recovered debris were provided in EXCEL files. Data on 75,440 pieces of recovered debris included impact coordinates. The total recovered weight was 84,900 lbs., approximately 38% of expected orbiter and payload landing weight. For 15,470 pieces of recovered debris at least two dimensions were provided. Most measurements did not include a third dimension. A histogram of estimated fragment areas is shown in Figure 2-4. The histogram exhibits the characteristics of an exponential distribution. In addition, an 800 lb turbo pump impacted with an estimated kinetic energy equivalent to 2 lb TNT (β = 300 lbs/ft^2 at terminal velocity $\approx$ 500 ft/sec). It will be seen later that the risk contributed by the turbo pump was very small compared to the risk from the large number of smaller fragments.

NASA provided material descriptions that allowed categorization of debris into material types: tile, tile & metal, metal, composite and fabric. This process was keyword driven. For example, "HRSI" and "FRCI" would identify a fragment as "High-Temperature Reusable Surface Insulation" or "Fibrous Refractory Composite Insulation Tiles" respectively [5]. Note, if it was both composite and metal, it was categorized as metal.

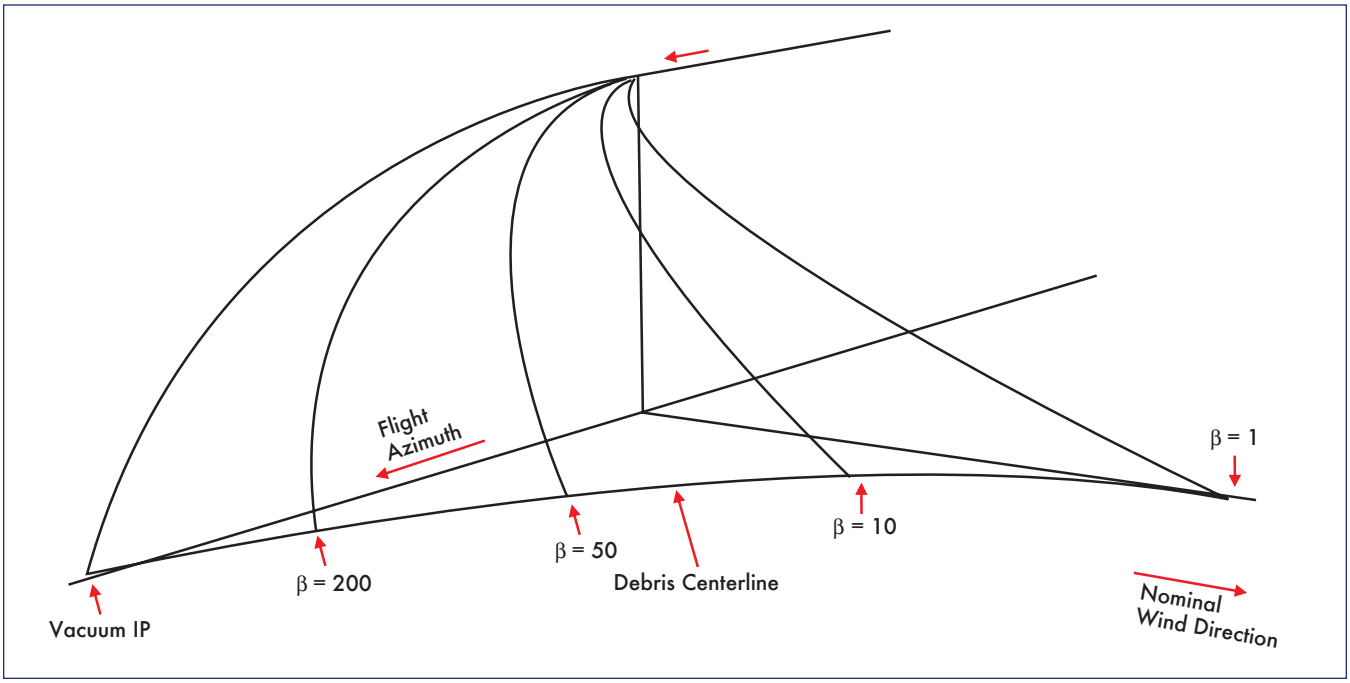

Figure 2-3. The Influence of the Ballistic Coefficient, β, and Wind upon Debris Impact Points.

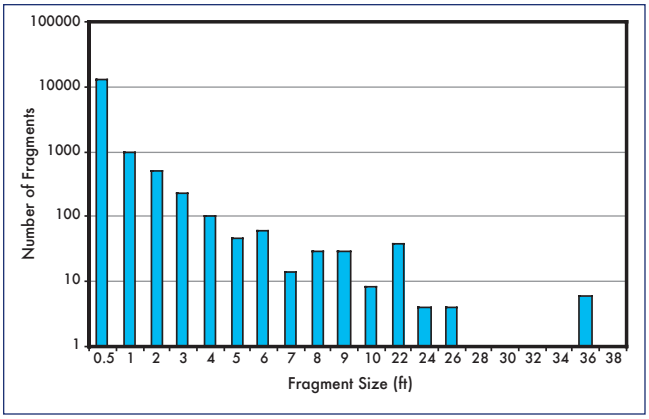

Figure 2-4. Size Histogram of Measured Fragments.

Figure 2-5 contains a flow chart of the rule-based algorithm used to estimate the dimensions and weight of each fragment. Table 2-1 contains the material densities. Several parameters used in these rules were varied to meet the constraint of overall weight. These parameters are the minimum and maximum plate thickness, and empty volume ratios F_1, F_2. (F_1 and F_2 are fractions of the volume defined by the exterior boundaries that contains no material).[2] Although the final values for the minimum and maximum plate thickness may seem unrealistically thin, it can be justified in part by the assumption that many plate fragments may be triangular instead of rectangular in shape and thus have a smaller mass

Material	*Density (lb/ft³)*
Steel	502
Aluminum	168
Graphite/Epoxy	124
HRSI Tiles	22
FRCI Tiles	12
LRSI Tiles	9
Insulation Fabric	9

Table 2-1. Material Densities.

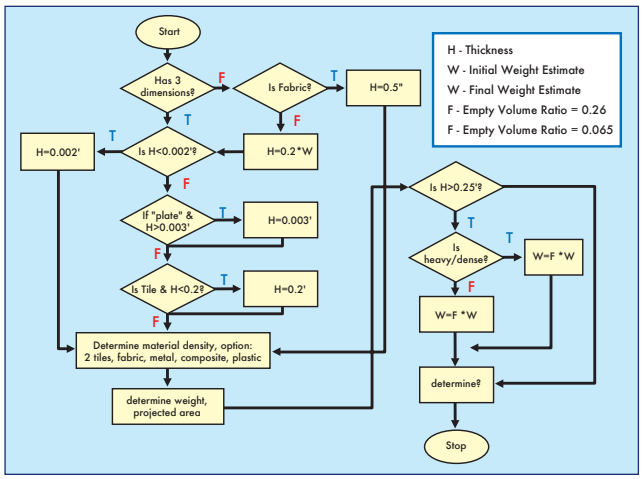

Figure 2-5. Rule Based β (Ballistic Coefficient) Approximation.

that would lead to a smaller thickness for an equivalent rectangular plate having the same length-width dimensions. A plate fragment may also have holes and non-uniform thickness. Furthermore, weight accuracy for individual fragments can be relaxed provided a reasonable weight distribution is found and the overall weight constraint is satisfied.[3] Figure 2-6 shows the β distribution of measured fragments. The distribution appears to be similar to a lognormal distribution with the mean located in the $1 < \beta < 3$ lb/ft^2 category.

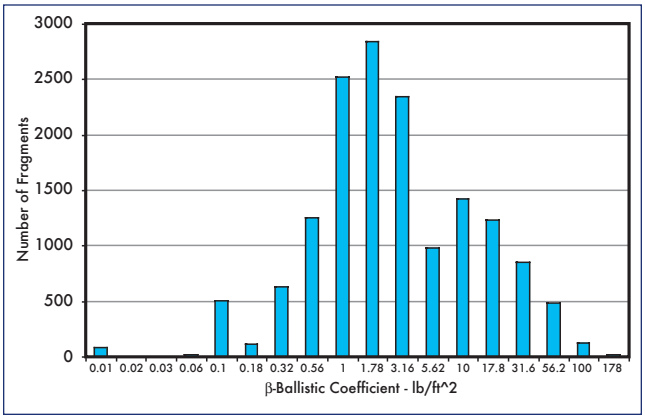

Figure 2-6. Debris List Extracted from Records with at Least Two Dimensions.

2.4 Development of Reference Trajectories

Initial positions and velocities for the reference trajectories were first based on the orbiter's last known state vector at loss of signal. A computer program, TAOS, was used to generate the base trajectories [6]. Each trajectory is configured to have the longest impact range for its debris. Some of the initial positions were subsequently modified to align the footprints with gathered data. For Group 1, the initial position was moved south by 3.2 miles. For Group 3 the initial position was moved south by 11 miles. Final trajectories for all four major fragment groups are plotted in Figure 2-7.

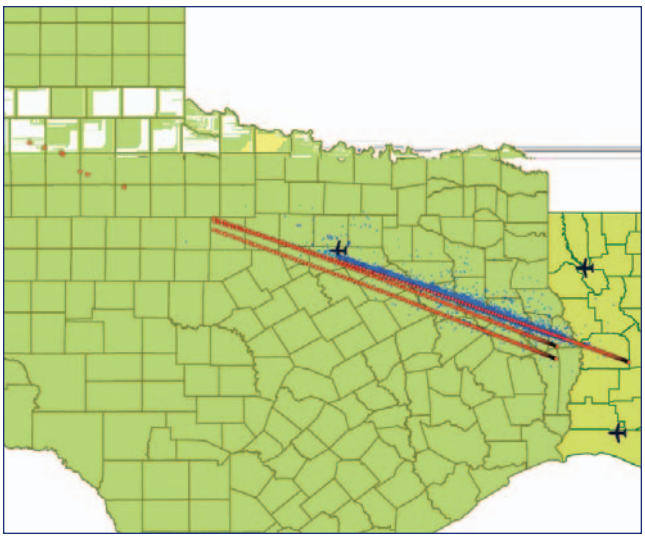

Figure 2-7. Reference Trajectories.

2.5 Development of Breakup State Vectors and Associated Debris Groups

The breakup state vectors are based on a progressive breakup model that initiated at 13:59:30 GMT and spans 120 seconds. 24 debris lists are created for each five-second interval. 5 state vectors are used to cover each five-second interval. Each state vector was assigned a failure probability of 0.2. In other words, each debris group is distributed evenly over a five-second span.

To populate the debris list, a trial run was used to determine the relationship of downrange distance and failure time for each ballistic coefficient, β class (see Figure 2-8). In this study, the Loss of Signal (LOS) point at -99.0413 °E, 32.956 °N is used as the point of origin. Next, the downrange impact distance for each fragment is measured from the same point of origin.

If the approximate size and dimension of a piece of debris were available, a ballistic coefficient is assigned and the relationship shown in Figure 2-8 is used to interpolate for the breakup (shedding) time for the fragment. Fragments without dimensions are assigned ballistic coefficients such that the ballistic coefficient distribution matches that of the fragments with dimensions at a similar downrange distance, and from this a breakup/shedding time. If there is not sufficient information to determine the breakup/shedding time by either of these two means, a low (i.e. 1.7 psf) ballistic coefficient is assigned with the condition that the final total weight of all fragment groups must be equivalent to the recovered weight of debris. Less than 10 percent of all the fragments belong in this category.

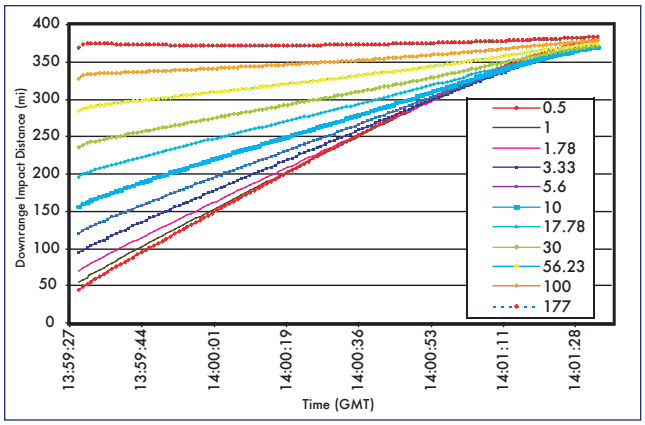

Figure 2-8. Relationship between Downrange Impact Distance and Downrange Time for each Ballistic Coefficient Group (Measured from Loss of Signal).

Figure 2-10 shows the debris model for group 1 for each ballistic coefficient class and breakup time. The ballistic coefficients used start at 0.5 lbs/ft^2 and increase logarithmically in quarter power increments up to 333 lbs/ft^2. Figure 2-11, Figure 2-12, and Figure 2-13 show the debris models for fragment groups 2, 3 and 4 respectively. When compared to other groups, group 4 fragments broke off earlier in the time frame.

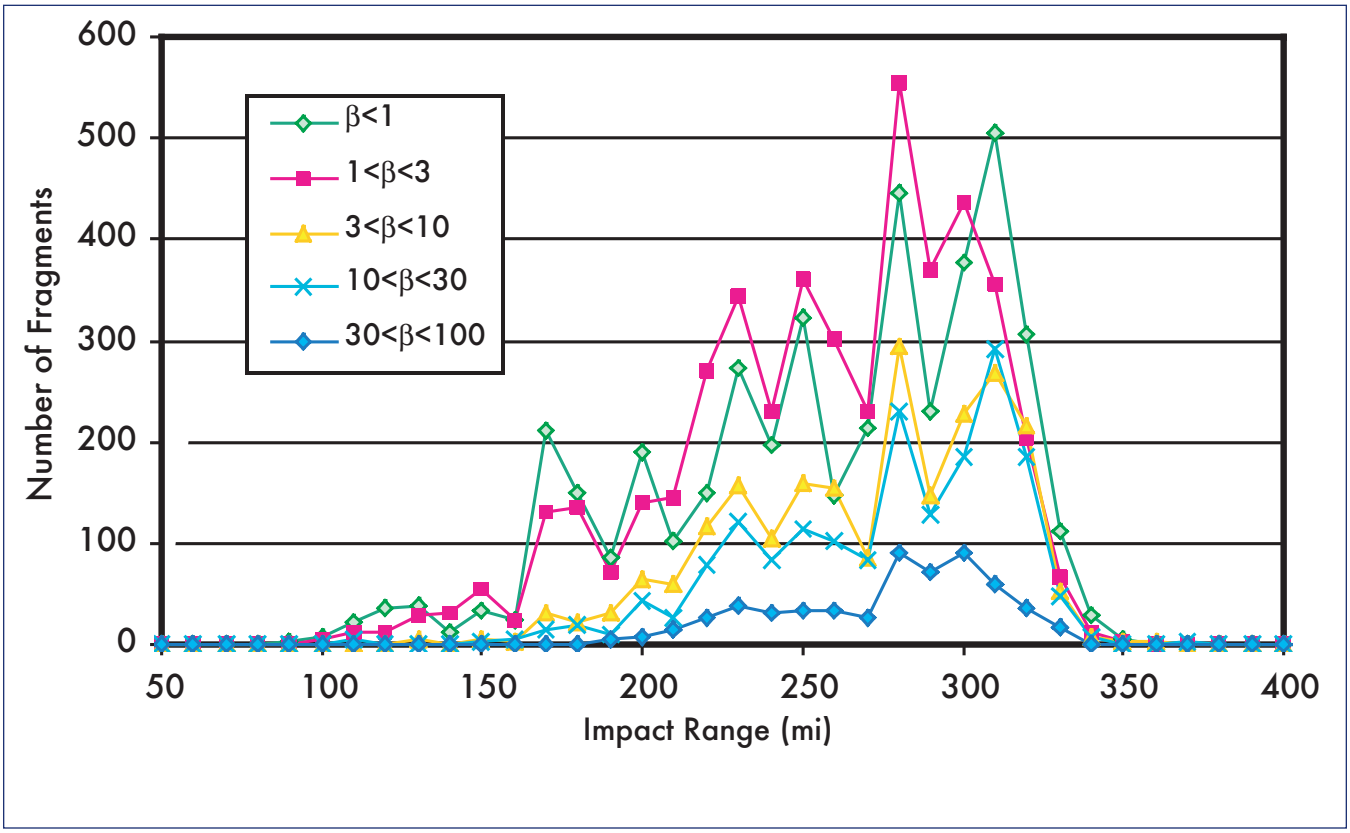

Figure 2-9. Distribution of Debris with Dimension Data as a Function of Impact Range.

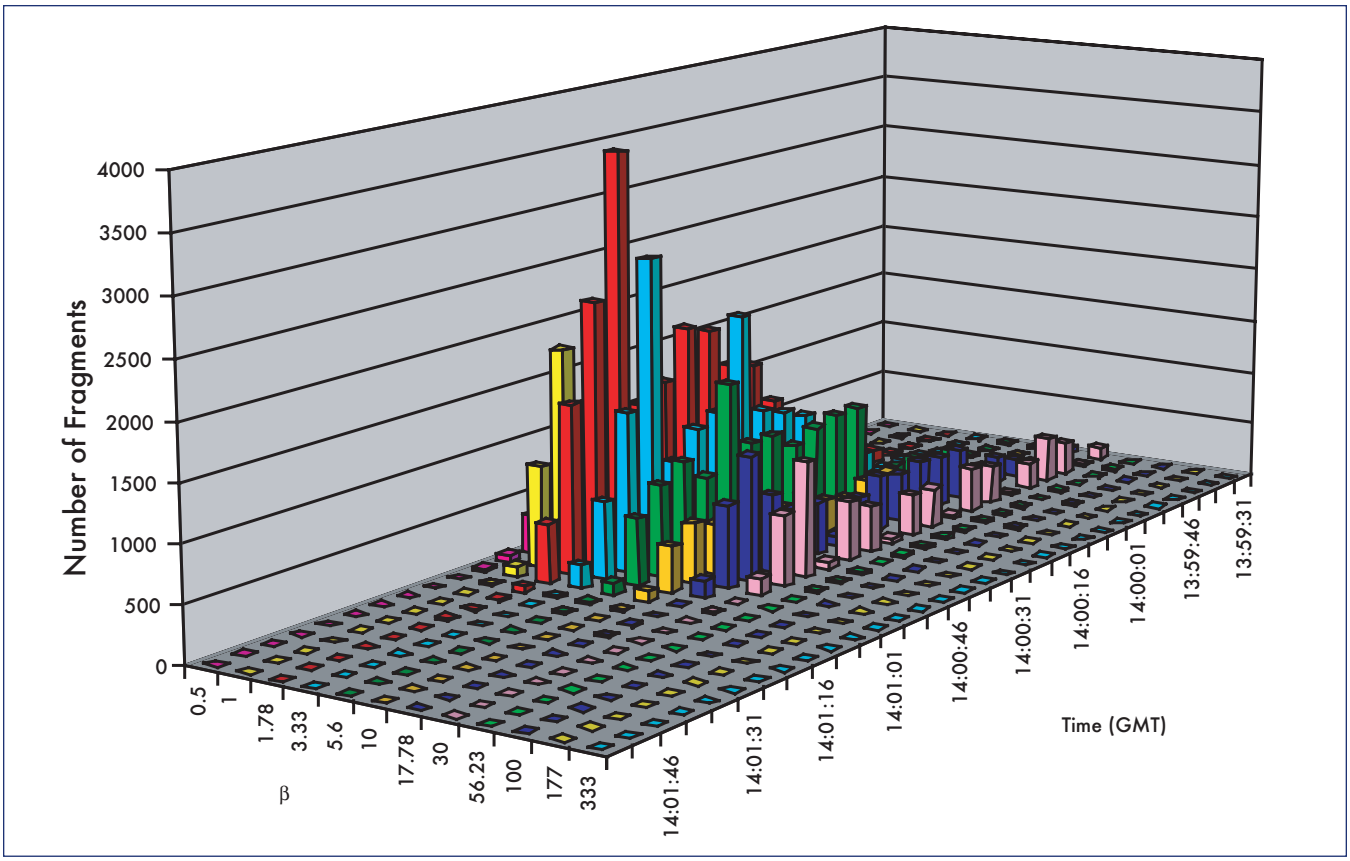

Figure 2-10. Group 1 Debris List.

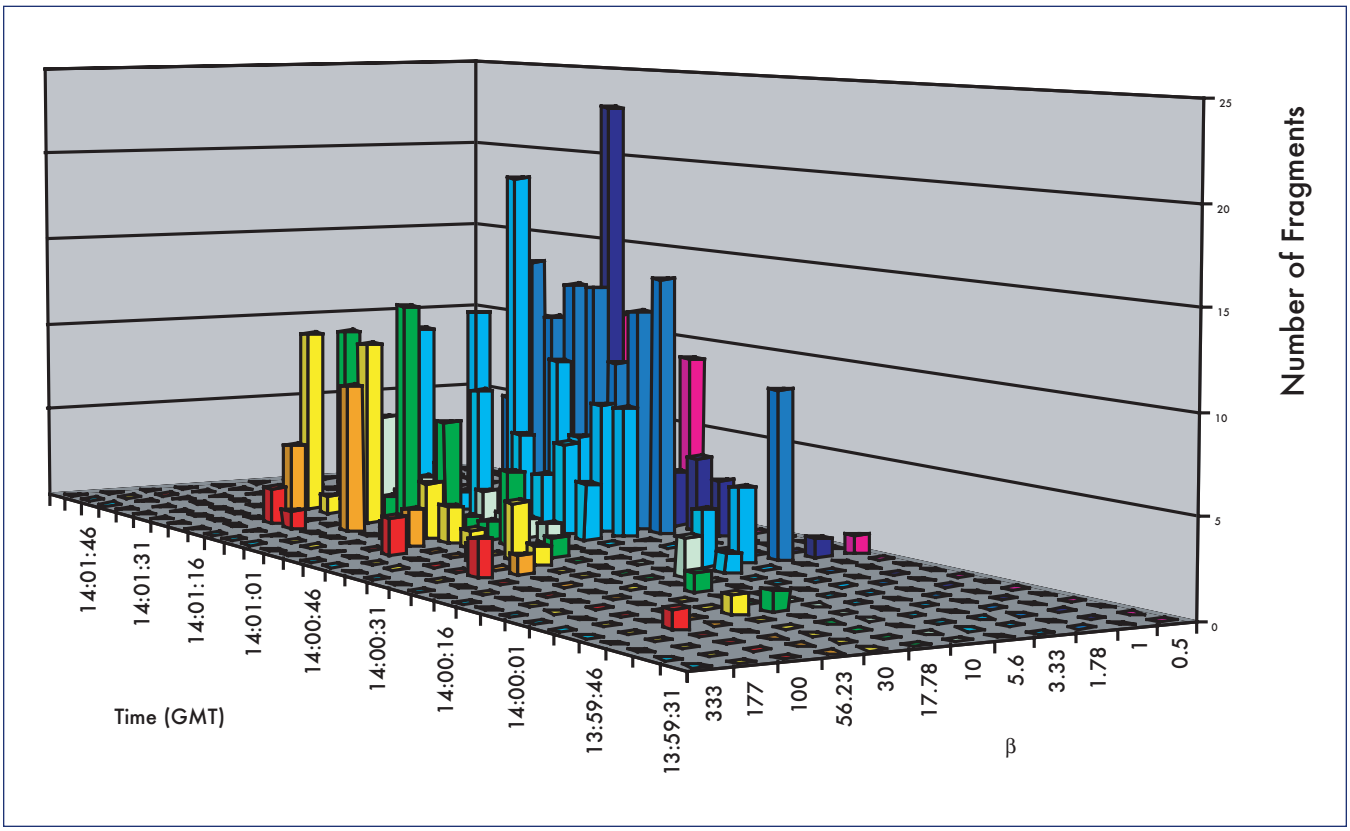

Figure 2-11. Group 2 Debris List.

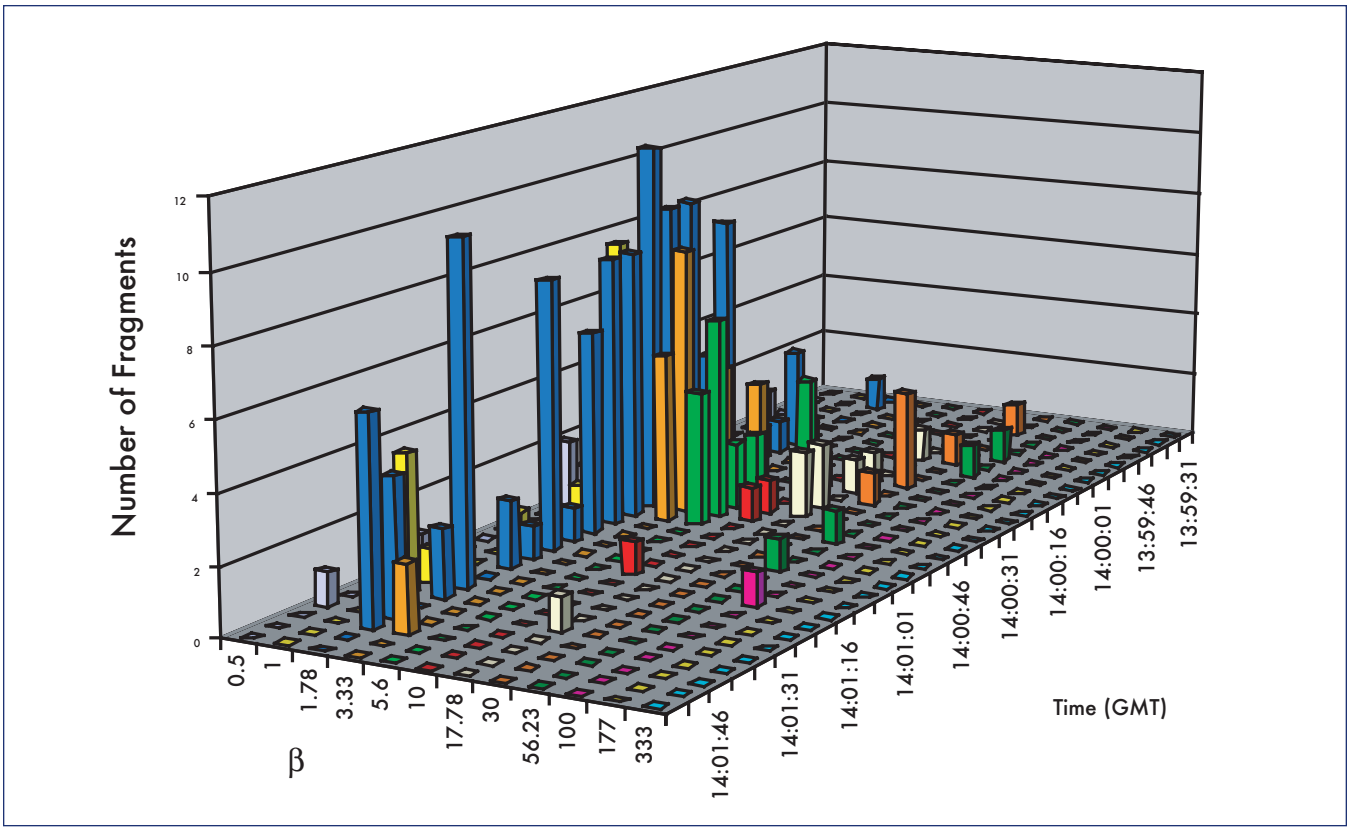

Figure 2-12. Group 3 Debris List.

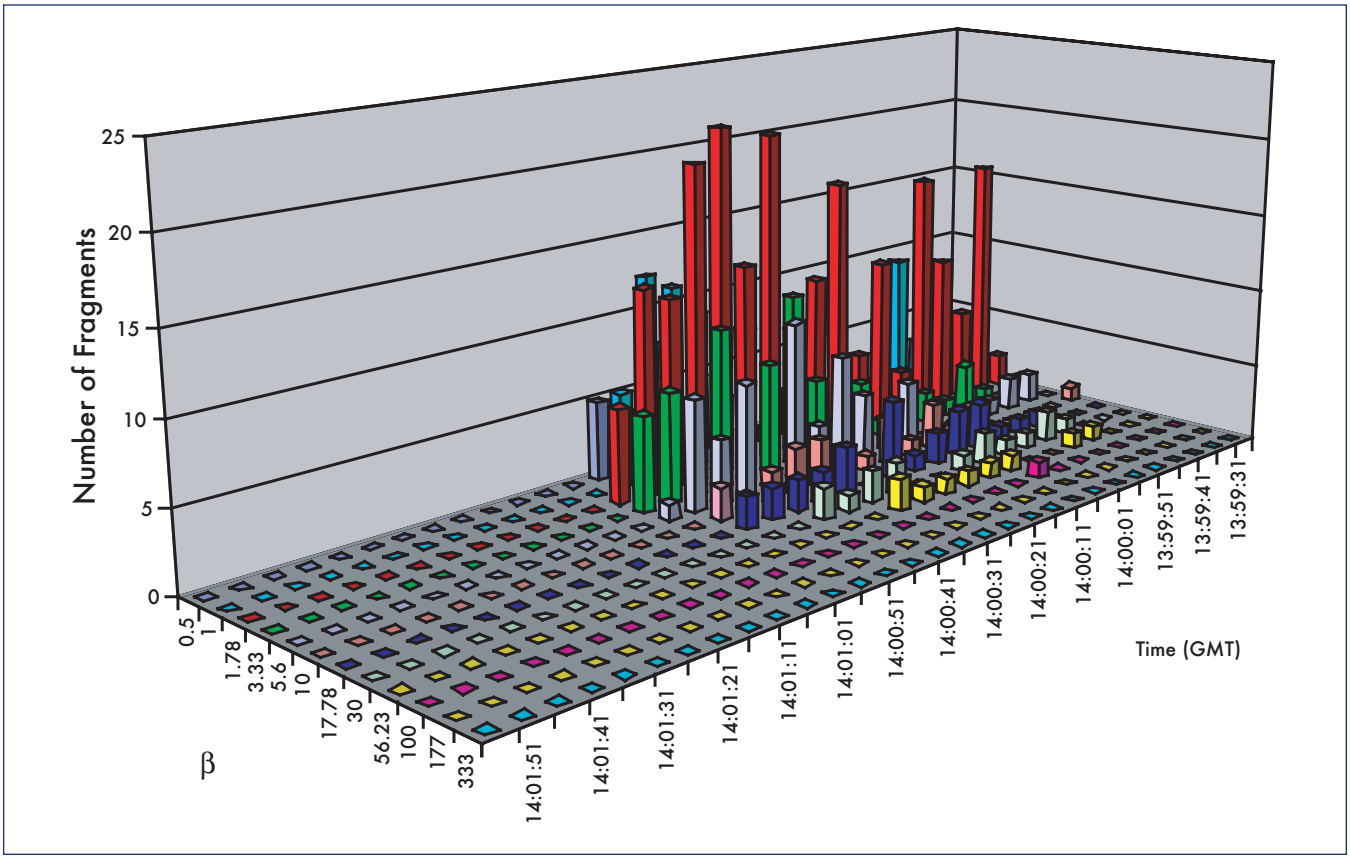

Figure 2-13. Group 4 Debris List.

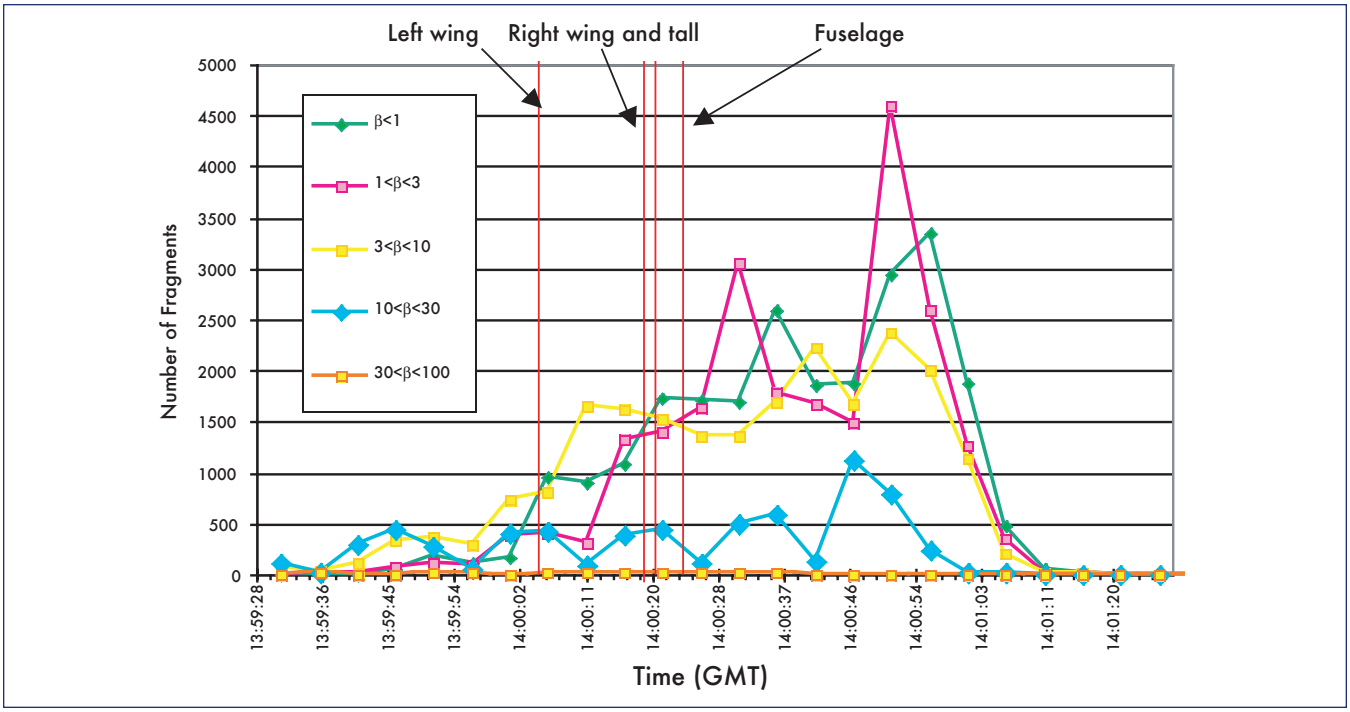

Figure 2-14. Estimated Breakup Model as a Function of Time by Ballistic Coefficient Category.

The breakup model developed to account for the total weight of the recovered debris is plotted in Figure 2-14. The fraction of the highest ballistic coefficient group $30<\beta<100$ lbs/ft^2 is much less prominent when compared to the impact range distribution shown in Figure 2-9 because the fragments without dimensions were not assigned to large weight debris groups in order to meet the overall weight constraint. Because the breakup model would vary if the reference trajectory is varied, it does not reflect the actual time when a fragment separated from the orbiter. It does, however, illustrate the progressive nature of the breakup process, and matches the available data as presented in Section 3.

3. Debris Dispersion

3.1 Basics of Impact Dispersion of Debris

The dispersion of debris impact location associated with a given initial state vector is illustrated in Figure 3-1. The primary sources in the case of the Columbia breakup are the ballistic coefficient, wind and velocity perturbation. The development of these uncertainties is explained in the technical paper describing CRTF included as Appendix A.

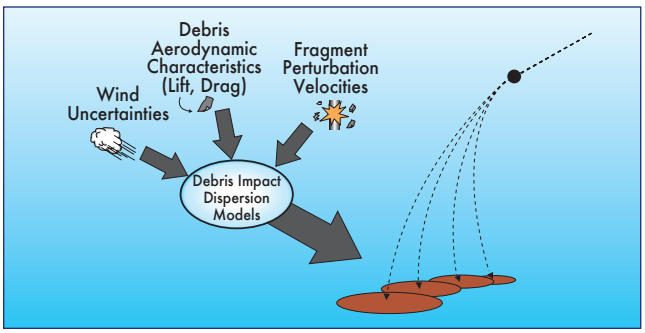

Figure 3-1. Contributions to Debris Dispersion Models.

3.2 Description of CRTF and RRAT

CRTF was developed to estimate the range of free-fall, the mean impact locations and impact dispersions of fragments resulting from a vehicle breakup. Either CRTF's dispersion footprints or the impact probability (P_I) contours can be used to define the hazard areas. CRTF can also define hazard areas as a moving volume in space, thereby providing means for assessing risks to aircraft.

3.3 Computed Dispersion of Debris Using the Breakup Model

Wind data for Feb 1, 2003 was obtained from both the Dallas/Fort Worth and the Shreveport airports. A monthly averaged model was used for atmospheric temperature and density, and for upper atmospheric winds. Probability of impact, P_I, per 1000 square feet for each of the debris group was contoured and is presented in Figures 3-2, 3-3, 3-4 and 3-5 for four debris groups. The combined contours are plotted in Figure 3-6. Figure 3-7 provides a three-dimensional view of the reference trajectories and combined P_I contours. Figures 3-8 and 3-9 compare the dispersion of the gathered debris and the model results in both the downrange and cross-range directions. The standard deviation used for the lift-to-drag ratio was 0.04 for all debris groups. This value produced the best fit to the cross-range dispersion of the debris in Group1. The standard deviation of velocity impulse in Groups 1 to 3 was assumed to be zero and in Group 4 was assumed to be 333 ft/sec respectively.

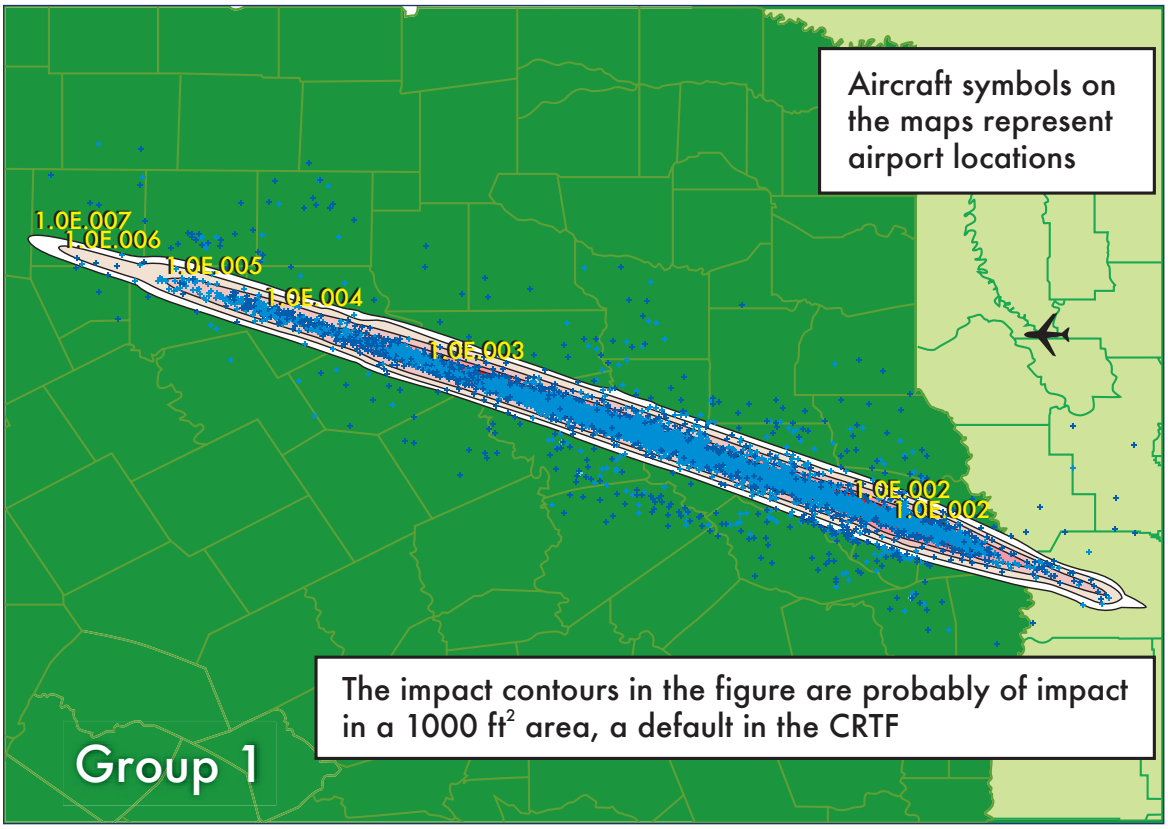

Figure 3-2. Comparison of Gathered Data with Modeled Dispersion (Group 1).

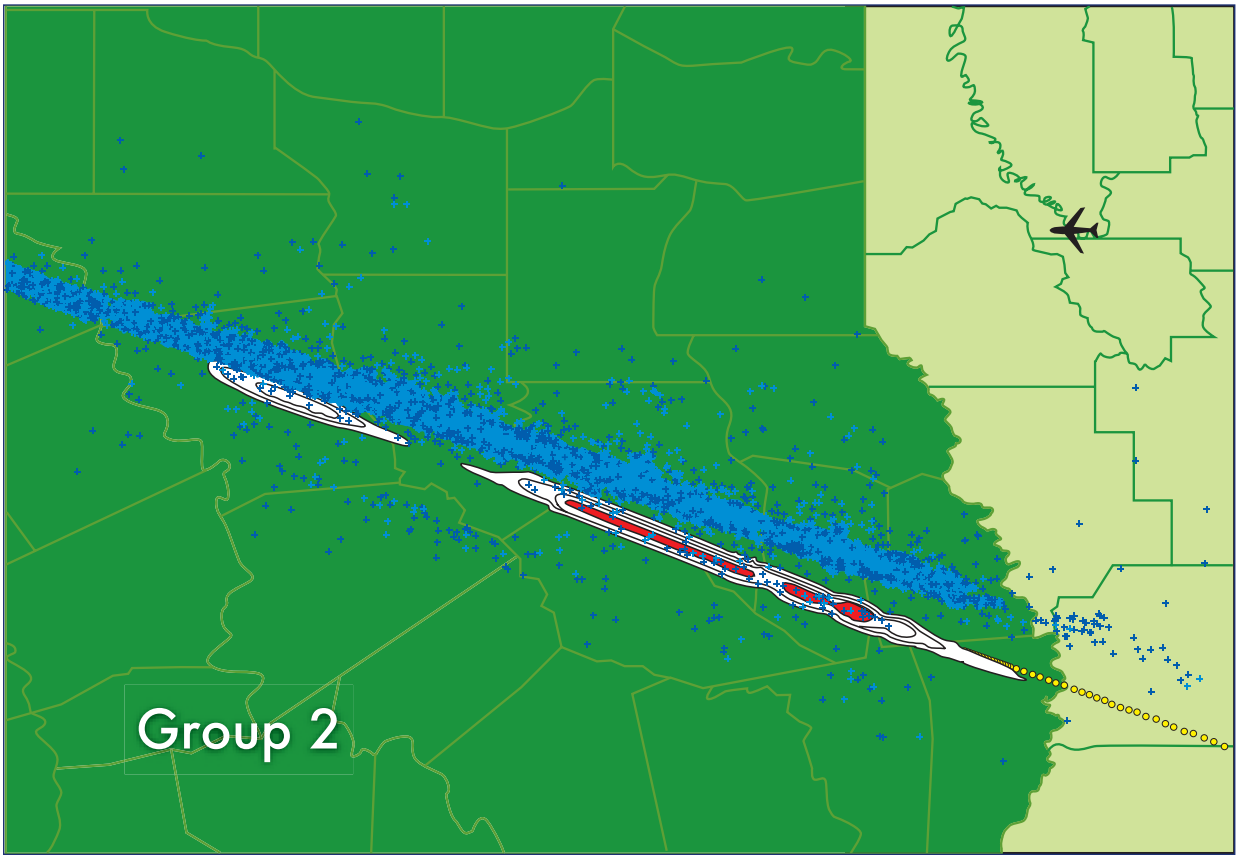

Figure 3-3. Comparison of Gathered Data with Modeled Dispersion (Group 2).

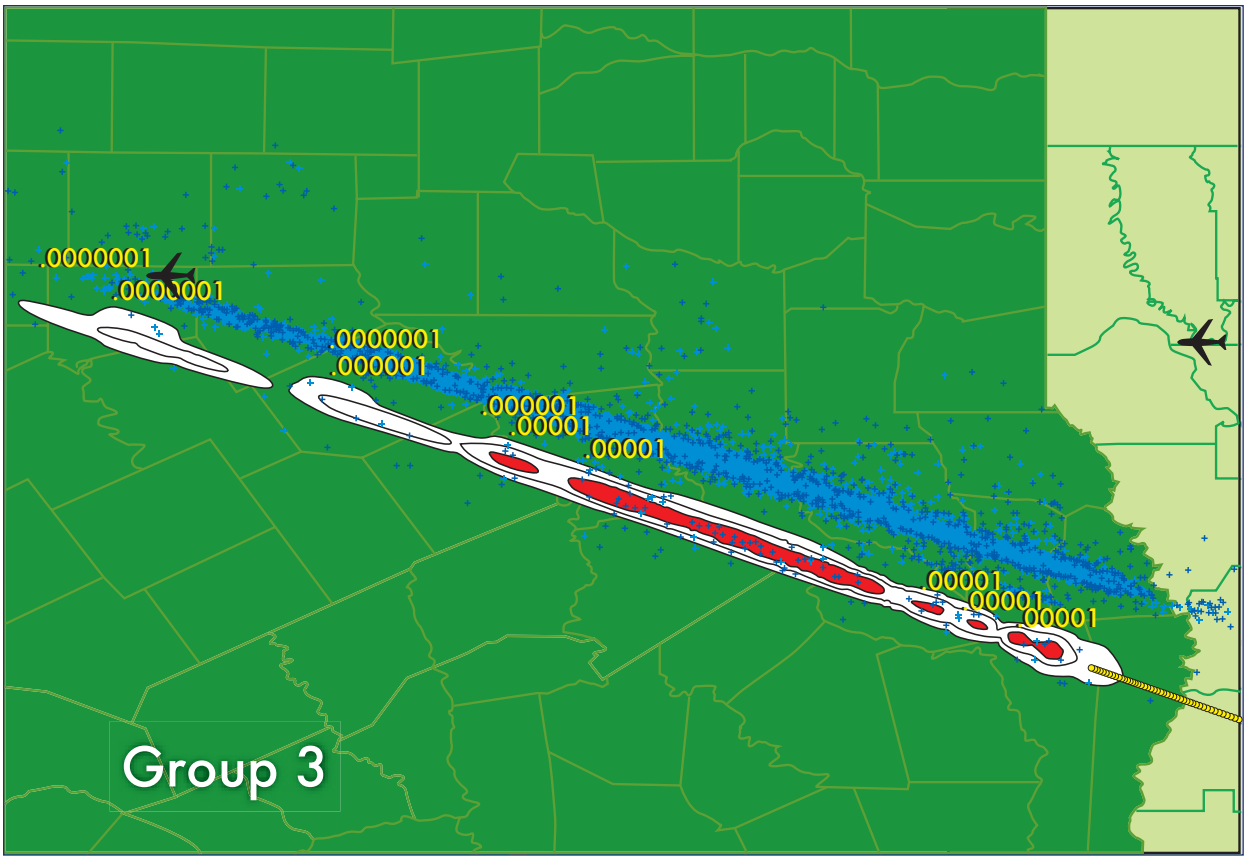

Figure 3-4. Comparison of Gathered Data with Modeled Dispersion (Group 3).

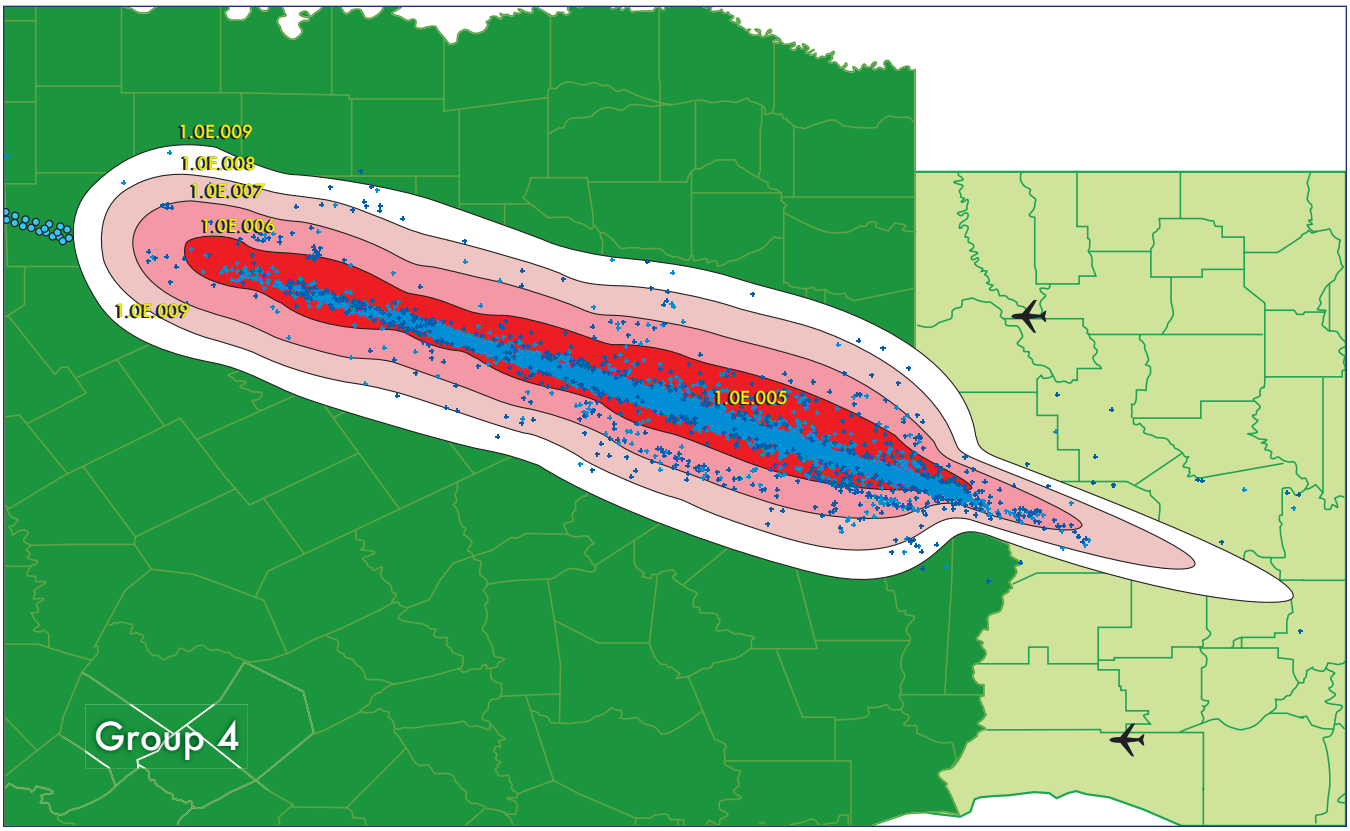

Figure 3-5. Comparison of Gathered Data with Modeled Dispersion (Group 4).

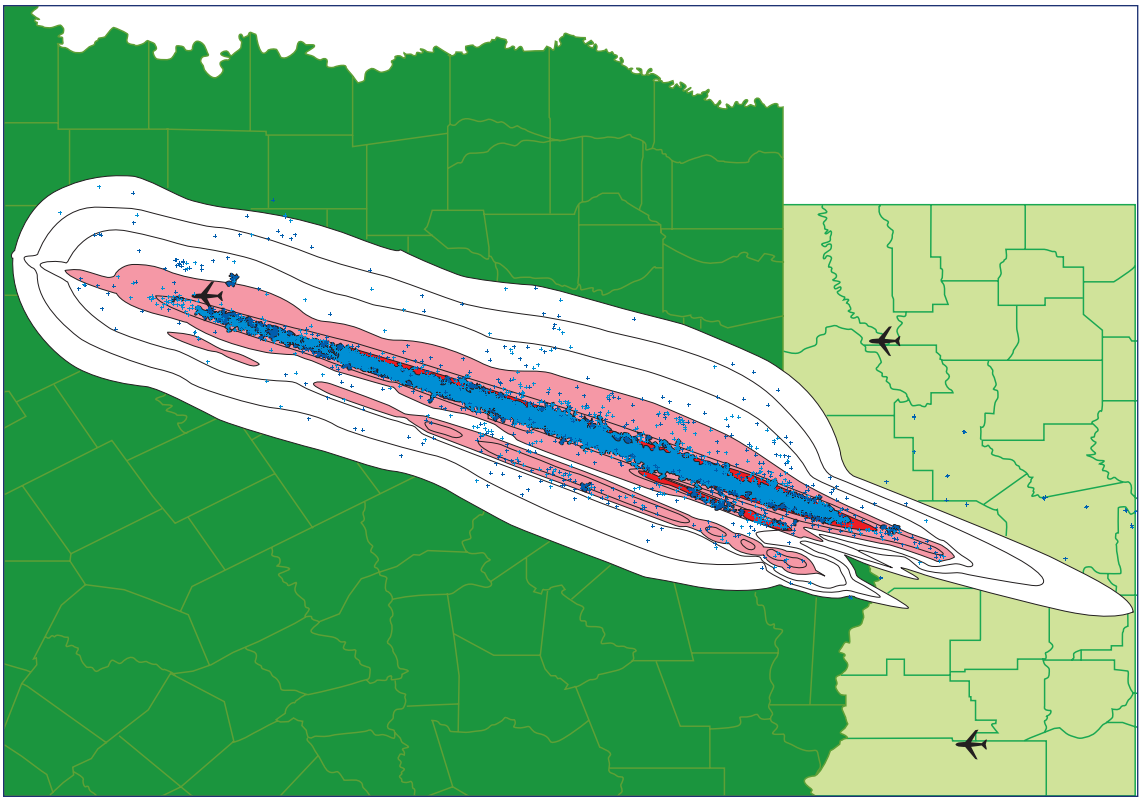

Figure 3-6. Comparison of Gathered Data with Modeled Dispersion (All Groups).

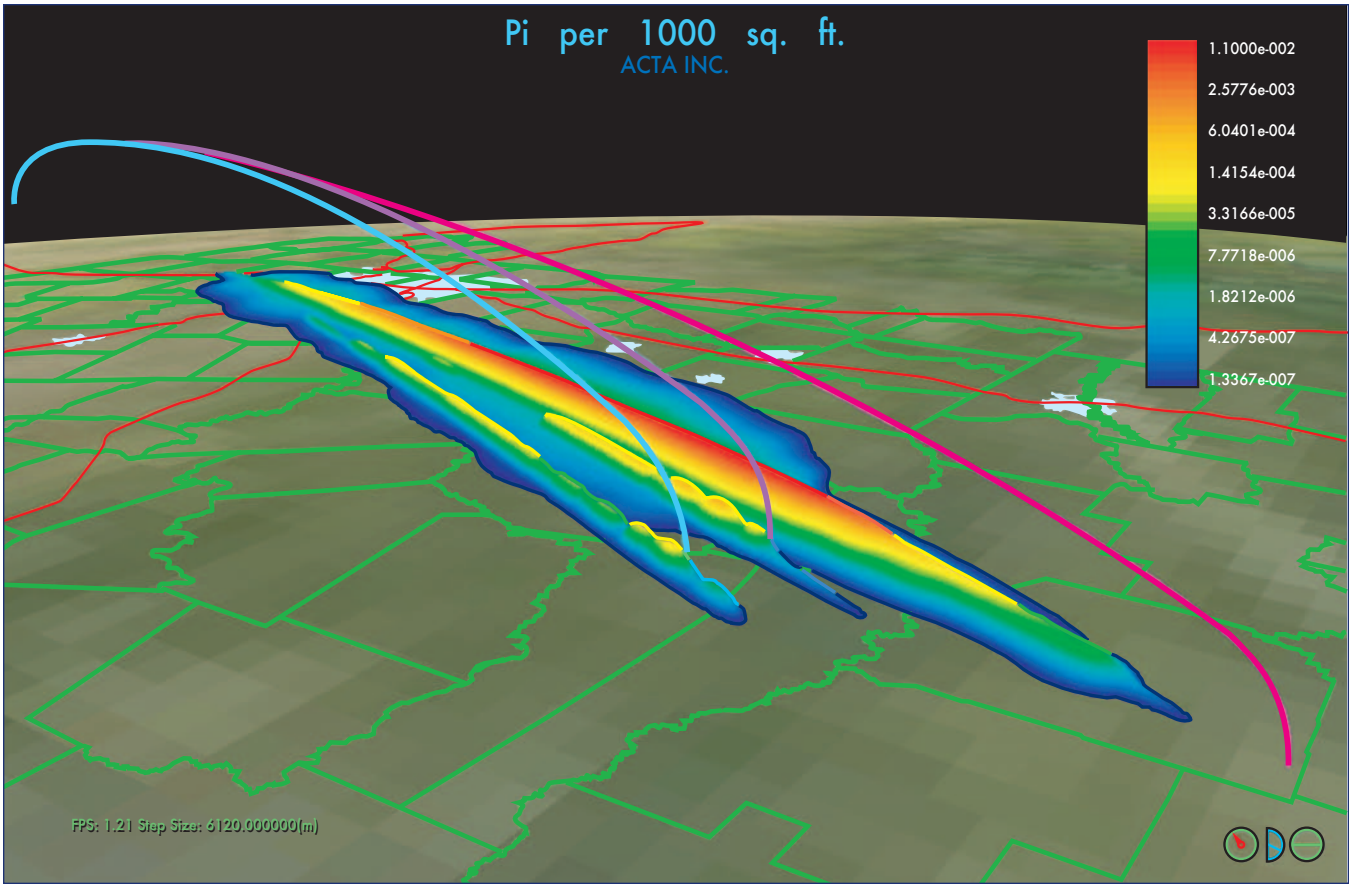

Figure 3-7. Modeled Debris Density in Three Dimensions .

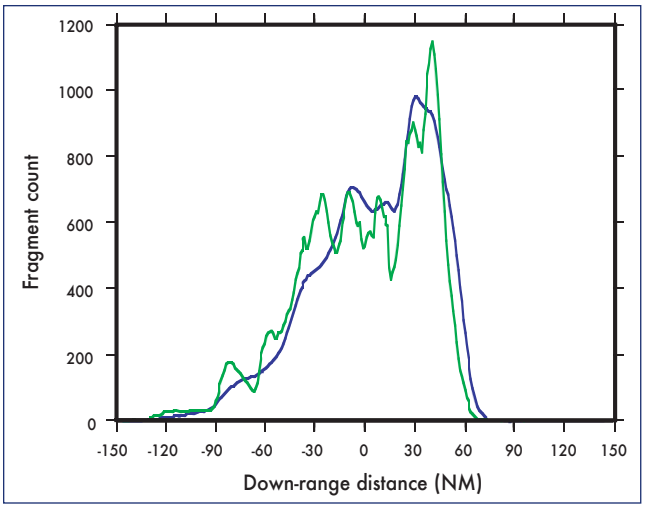

Figure 3-8. Comparison of the Actual Fragment Count (Green) in the Downrange Direction with the Fragment Count in the Reconstructed Model (Blue).

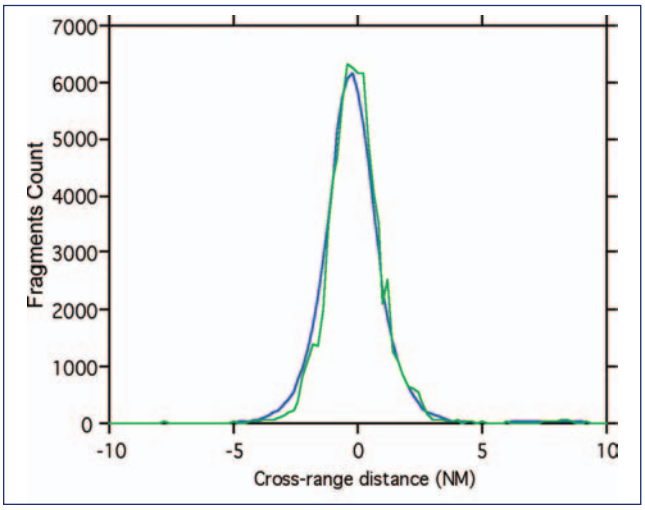

Figure 3-9. Comparison of the Actual Fragment Count (Green) in the Crossrange Direction with the Fragment Count in the Reconstructed Model (Blue).

4. Casualty Model Due To Debris Impacting On People In The Open

4.1 Basic Impact Casualty Model

The estimated threat to people in the open from Columbia debris impacts took into consideration:

1. the angle of impact and of the debris (it is not vertical if there is a ground wind),
2. the possible effect of bounce, roll or secondary breakup,
3. the vulnerability of the body to debris impact.

Table 4-1 gives a summary of the six Abbreviated Injury Scale (AIS) levels from minor to virtually unsurvivable. The AIS scale is used as a measure of severity of injury for individuals arriving at hospital emergency rooms. The term casualty in this study applies to all individuals predicted to sustain an injury that is at AIS level 3 or higher (including fatality). The serious injury level was chosen because it is consistent with the severity levels used by the FAA and the Air Force Eastern and Western Ranges for launch vehicle risk assessments.

AIS Level	Severity	Type of injury
0	None	None
1	Minor	Superficial
2	Moderate	Reversible injuries; medical attention required
3	Serious	Reversible Injuries; hospitalization required
4	Severe	Life threatening; not fully recoverable without care
5	Critical	Non-reversible injury; not fully recoverable even with medical care
6	Virtually Unsurvivable	Fatal

Table 4-1. Abbreviated Injury Scale (AIS).

Figure 4-1 presents the median delineating the region of casualty producing impacts as a function of fragment weight and impact velocity. Note the three injury mechanisms that depend on weight and impact velocity. There is considerable inherent uncertainty in any casualty estimate because the level of injury produced by an impact depends on a variety of factors including the body part impacted, the weight, age and health of the person impacted, as well as the characteristics of the fragment. Thus, in the model, the line separating casualty from non-casualty has an uncertainty represented by a probability density function. These uncertainties are included in the CRTF casualty model used here. The models are based on simulations of actual impacts on dummies with the dummy responses being numerically modeled by a biomechanical computer program to compute different AIS levels.

The casualty area is a primary parameter in the risk computation. The casualty area is the equivalent impact area that will lead to a casualty if a person is struck by a piece of debris with sufficient weight and velocity to cause the person to become a casualty. If the debris is falling vertically, the casualty area is estimated by first taking the maximum projected area of the piece of debris, finding the equivalent radius of the piece and then adding a foot to the radius to represent the radius of the equivalent human. The basic casualty area, A_c, in square feet, for vertical impact is then expressed as

$$A_c = \pi \left(\sqrt{\frac{A_f}{\pi}} + 1 \right)^2 \qquad (4\text{-}1)$$

where A_f is the maximum projected area of the fragment in

square feet.

If a fragment has a horizontal component of velocity, then the velocity and weight must also be evaluated to determine if a person can become a casualty due to being hit horizontally in the head, thorax, abdomen or legs. A vulnerability model is necessary for each of these cases such as that in Figure 4-1. Currently CRTF contains models for the head, thorax and abdomen but not for legs. The abdomen model was extended down to the ankles in this study. As will be seen, the horizontal velocity component does not contribute much in this study because the combined weights and horizontal velocities are rarely sufficient to produce a casualty.

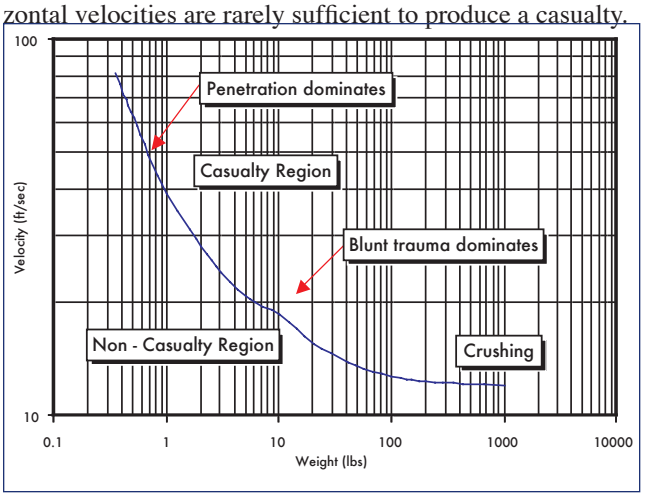

Figure 4-1. Relationship between Casualty (AIS 3) and Fragment Impact Conditions.

If the fragment has a horizontal velocity, and does not directly strike the person, it can bounce, skid or roll and then strike the person. These aspects are also in the CRTF casualty model with the logical treatment illustrated in Figure 4-2. The casualty area for the horizontal component of velocity now uses the height and width of a person with the effective radius of the fragment, $\sqrt{(A_f/\pi)}$, added to the dimensions on three sides. The expanded casualty area accounts for potential hits on the head, thorax and abdomen with separate vulnerability models for each of these body parts. The potential for bounce, skid and roll is strongly dependent upon the firmness of the ground and on the material properties and shape of the impacting fragment. In addition, casualties can result from breakup of the fragment upon impact, especially for high velocity fragments. Because very few fragments from Columbia appeared capable of significant breakup after impact, this effect was not considered in this study.

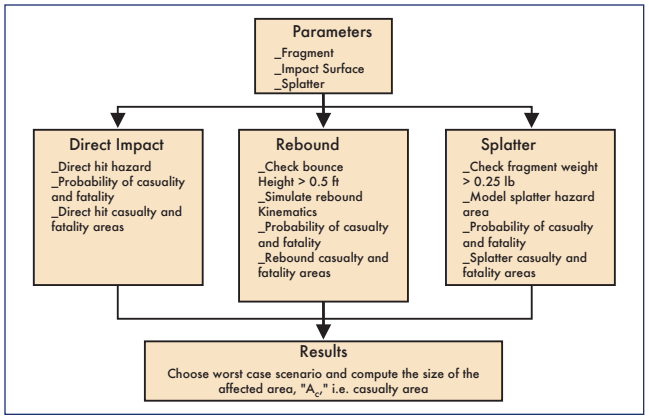

Figure 4-2. General Logic for Computing Casualty Area.

This study assumes that everyone in the open is standing. At eight o'clock in the morning, few are expected to be lying down or sitting, outside. If these positions must be considered, then the CRTF casualty model can be adjusted accordingly.

4.2 Casualty Areas for Representative Debris

Casualty areas, using the logic described in Section 4.1, were computed for all of the debris classes in Figure 2-4. These are presented in Table 4-2 on the next page. Hazard area and fatality area are computed as well. The hazard area covers all cases of impact without injury, non-fatal injury and fatal injury. In addition, the numbers of fragments in each category are included, enabling the computation of total hazard area, casualty area and fatality area.

Notes:

1. The debris list used here is the result of the process of scaling up and adjustment of the debris described in Section 2. This is the same debris list as the one used in the more detailed analysis.
2. Assumed 10 ft/s surface wind, drag coefficient = 0.6, coefficient of restitution = 0.25, kinetic friction coefficient = 0.6, rolling friction coefficient = 0.06.
3. Fragment Category 11 had one high velocity fragment that reportedly did not break on impact (splatter). For purposes of the study, it was assumed that the mechanical energy of impact was converted to TNT (2 lb) and used the overpressure and impulse on the human body to determine equivalent hazard, casualty and fatality areas. The effect of this assumption does not influence the final result because there was only one fragment in this category.

Figure 4-3 contains a histogram showing the distribution of total hazard, casualty and fatality areas among the debris classes.

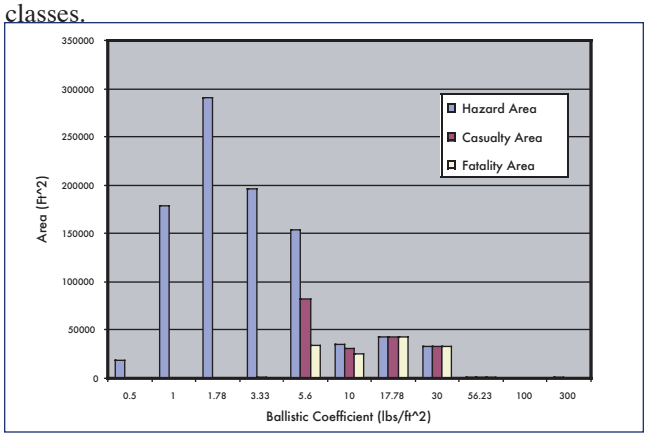

Figure 4-3. Distribution of Total Hazard, Casualty and Fatality Area among the Debris Classes.

	Wf	Af	Beta f	Vf	Theta f	KE f	N		A haz	A cas	A fat	A haz	A cas	A fat
	(lb)	(ft^2)	(lb/ft^2)		(deg.)	(lb-ft)			(ft^2)	(ft^2)	(ft^2)	(ft^2)	(ft^2)	(ft^2)
Frag. Cat.	Ave. Frag. Wt.	Ave. Frag. Area	Ballistic Coeff.	Impact Velocity	Impact Angle	Kinetic Energy	No. of Frags.	Total Wt.	Hazard Area	Casualty Area	Fatality Area	Total Hazard Area	Total Casualty Area	Total Fatality Area
1	0.04	0.143	0.50	22.9	25.9	0.3	1860	80	10.3	0.0	0.0	19160	0	0
2	0.19	0.312	1.00	30.8	19.0	3	11260	2106	15.9	0.0	0.0	179348	0	1
3	0.22	0.204	1.78	40.1	14.4	5	19541	4260	14.9	0.0	0.0	290452	6	8
4	0.37	0.185	3.33	54.0	10.7	17	13846	5109	14.1	0.1	0.0	195888	692	68
5	1.32	0.392	5.60	69.6	8.3	99	10901	14357	14.1	7.6	3.1	154141	82779	33765
6	1.77	0.295	10.00	92.6	6.2	236	4597	8146	7.7	6.8	5.5	35318	31148	25453
7	2.63	0.247	17.78	123.1	4.7	620	6969	18356	6.1	6.1	6.1	42758	42758	42758
8	5.04	0.280	30.00	159.7	3.6	1995	5387	27140	6.1	6.1	6.1	32665	32665	32665
9	9.67	0.287	56.23	218.4	2.6	7166	246	2379	5.9	5.9	5.9	1448	1448	1448
10	4.29	0.072	100.00	291.2	2.0	5648	33	142	4.5	4.5	4.5	150	150	150
11	800	4.444	300.00	504.1	1.1	3157056	1	800	1017.9	113.1	15.4	1018	113	15
Total for all fragments							74641	82874				952346	191760	136332

Table 4-2. Hazard, Casualty and Fatality Areas for People in the Open Based on Recovered Columbia Debris.

5. Exposure And Sheltering Model

The exposure model provides numbers and locations of people at risk on the ground to the impacting debris, and location and density of flying aircraft in the vicinity of the debris during descent. The model of people on the ground considers those both inside and outside of structures and vehicles. In addition, it provides the degree of sheltering offered by roofs and upper floors for categories of structures most likely in the region of debris impact. This is typically called a "population model with sheltering," and this study provides a population model with sheltering for all of Texas and Louisiana, encompassing the area where debris from the *Columbia* was recovered. The probability of impact to aircraft is typically much smaller than the risk to people on the ground, as found in the study of the risks of a return from orbit of a generic lifting entry vehicle [7]. To make an initial approximate estimate of the effects of the debris on aircraft in flight due to this event, an aircraft model was used that is based on the work in a previous unrelated study. This section discusses the details of both the ground and the aircraft model.

5.1 Ground Exposure Methodology

Census data typically provides a reasonably high resolution model of the location of residences. However, it does not provide direct information about structure types needed to estimate sheltering characteristics. It is not cost-effective to survey a large region to determine the types of buildings present. One solution has been to arbitrarily assume a distribution of building types (typically only a couple of types) that applies across the whole region. This type of model usually has little justification, and is obviously not very reliable. Instead, we developed a modeling method that uses "proxy" data, and allows for variation among different places on a very fine scale.

The sheltering model development used four types of data: people counts (i.e. census), demographic/economic statistics, structural/engineering reports or knowledge, and georeferencing information (association of coordinates with named places). For a risk analysis, the resulting database must include three components: a quantitative geographic description of where people are located, a description of the structure types that provide protection to the population, and an allocation of how many people are in each structure type. These all must be in a format and a resolution convenient for risk analysis.

As intermediate steps, a population model (without sheltering), a model of sheltering percentages for each demographic group, and a model of sheltering percentages for each geographic region are developed. The model assumes that a more accurate model of structure types can be developed for a specific demographic category than for everyone at once. The process is outlined in Figure 5-1, where arrows indicate data flow, and double lines indicate linked data elements.

The primary challenge is to develop translations of the demographic information into distributions of people among

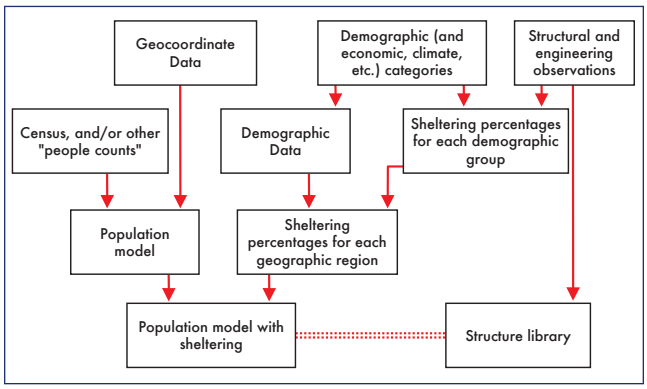

Figure 5-1. Population / Sheltering Modeling Overview.

sheltering types. At a top level, it is assumed that people are always in one of four locations: home, school, in transit [i.e. in cars], or work. The demographic data defines how many people are in each location. In addition, the demographic data for each category typically has some additional information regarding people in each location. For example, typical data for people at work is their occupation. The sheltering percentages are then modeled for each of these data items. For example, it might be assumed that people who are "gardeners" are outside 80% of the time and inside a one-story wood-roof structure 20% of the time during daylight hours. Other occupations have different sheltering distributions. A key assumption of the method is that better estimates of sheltering can be determined by occupation than for generic "working people".

Next, the percentage of people in each occupation is multiplied by the structure distribution for the occupation, and these percentages are summed over structure types. Mathematically, this is a matrix multiplication,

$$\begin{pmatrix} c_1 \\ c_2 \\ \vdots \\ c_m \end{pmatrix} = \begin{pmatrix} O_{11} & \cdots & O_{1n} \\ \vdots & \ddots & \vdots \\ O_{m1} & \cdots & O_{mn} \end{pmatrix} \begin{pmatrix} o_1 \\ o_2 \\ \vdots \\ o_m \end{pmatrix} \qquad (5\text{-}1)$$

where the vector **o** is the percentage of people in each occupation, each row of the matrix **O** has the distribution of structures for an occupation, and the vector **f** is the percentage of people in each structure class. A similar operation is performed for people at home and at school.

Estimating the number of people who are home, work, or school is complicated somewhat because these numbers change with time of day and season. For example, people are usually at work during the day and at home at night. In addition to the day/night difference, two factors differentially locate people: the time of year (especially for students) and weekday/weekend differences. There is little information available regarding these parameters, but reasonable assumptions can be applied to determine how these variations affect the resulting population model with sheltering. For this study, a model appropriate for daytime during a

winter weekend is appropriate. The scenario is implemented in the method by adding four parameters: the percentage of employed people who are actually at work, the percentage of students who are at school, and the percentage of people who are at home but instead are outside, and the percentage of people in transit.

The full method can be summarized by a matrix equation. The sheltering in a population center, **c** (a vector whose elements are the number of people in the sheltering categories), is calculated by:

$$\mathbf{c} = p\{e\mathbf{O}\mathbf{o} + s\mathbf{s} + (1-e-s)[(1-d)\mathbf{H}\mathbf{h} + (0 \quad 0 \quad \cdots \quad d)^T]\}, \tag{5-2}$$

where the "people in the open" structure category is the last element of vector c, and the variables are listed in Table 5-1.

The shelter types for people at work and school are distinguished from those at home. Census data provides detailed information about the prevalence of various types of residential structures, but this detailed data is not provided for non-residential structures.

Variable name	*Description*
p	Population in a given population center
d	Percentage of people at home who are outside (1-d is the percentage of people at home who are inside)
s	Percentage of people in school
e	Percentage of people at work
o, a vector elements o_{ij}	Percentage of people who are at work who are in each occupation category
O, a matrix elements O_{ij}	Percentage of people in each occupation category who are assigned to each sheltering type
s, a vector elements s_{ij}	Percentage of students in school who are assigned to each sheltering type
h, a vector elements h_i	Percentage of housing units in each housing structure category
H, a matrix elements H_{ij}	Percentage of each housing structure category which are assigned to each sheltering type

Table 5-1. Variables for Modeling Sheltering.

For clarity, the equation can be written with expanded notation as:
where there are *i* sheltering categories, *j* occupational categories, and *k* housing structure categories.

Consider a simple example: assume that all people at risk are working and that there are only two occupation categories, office workers and farmers. Also, assume that office workers are always in buildings, and may be in light, medium or heavy sheltering with equal probability (33% in each). Farmers, on the other hand, are usually outside, say 75 percent of the time, and in light structures the remaining 25 percent of the time. If there are 1,000 people in the population center, and 40 percent of the people are farmers and 60 percent are office workers, then the following equation characterizes the sheltering distribution:

$$\begin{pmatrix} c_{Light} \\ c_{Medium} \\ c_{Heavy} \\ c_{Open} \end{pmatrix} = \underset{\text{people}}{1000} \left\{ \begin{pmatrix} 100\% \\ \text{at work} \end{pmatrix} \left(\begin{array}{c|cc} & \textit{Office} & \textit{Office} \\ \hline \textit{Light} & 33\% & 25\% \\ \textit{Med} & 33\% & 0\% \\ \textit{Heavy} & 33\% & 0\% \\ \textit{Open} & 0\% & 75\% \end{array} \right) \begin{pmatrix} 60\% \text{ office} \\ 40\% \text{ farmers} \end{pmatrix} \right\} \tag{5-4}$$

which results in:

c_{Light} = 1,000 * 100% * (33% * 60% + 25% * 40%) = 300 people in light structures,
c_{Medium} = 1,000 * 100% * (33% * 60% + 0% * 40%) = 200 people in medium structures,
c_{Heavy} = 1,000 * 100% * (33% * 60% + 0% * 40%) = 200 people in heavy structures, and
c_{Open} = 1,000 * 100% * (0% * 60% + 75% * 40%) = 300 people in the open.

In this study, there are many more occupations and structure categories than in the example.

5.2 Sheltering Categories

The sheltering model allocates people to buildings, vehicles or to being in the open. Building/ vehicle roofs and building sub-floors provide some level of protection to their occupants from inert debris. ACTA previously developed inert debris roof/floor penetration models [8,9,and 10]. Table 5-2 shows the inert debris roof categories. For most roof types, there are three levels or protection: one for people on the top floor, one for people one floor lower, and one for everyone farther from the roof.

Figure 5-2 shows an example of the level of protection provided by several roof classes. The figure depicts the casualty area of a cubic steel fragment impacting face-on at terminal velocity as a function of fragment weight. The casualty area is the statistically expected area within which

$$\begin{pmatrix} c_1 \\ c_2 \\ \vdots \\ c_i \end{pmatrix} = p\left\{ e \begin{pmatrix} O_{11} & O_{12} & & O_{1j} \\ O_{21} & O_{22} & \cdots & O_{2j} \\ \vdots & \vdots & \ddots & \vdots \\ O_{i1} & O_{i2} & \cdots & O_{ij} \end{pmatrix} \begin{pmatrix} o_1 \\ o_2 \\ \vdots \\ o_j \end{pmatrix} + s \begin{pmatrix} s_1 \\ s_2 \\ \vdots \\ s_i \end{pmatrix} + (1-e-s) \left[(1-d) \begin{pmatrix} H_{11} & H_{12} & & H_{1k} \\ H_{21} & H_{22} & \cdots & H_{2k} \\ \vdots & \vdots & \ddots & \vdots \\ H_{i1} & H_{i2} & \cdots & H_{ik} \end{pmatrix} \begin{pmatrix} h_1 \\ h_2 \\ \vdots \\ h_k \end{pmatrix} \begin{pmatrix} 0 \\ 0 \\ \vdots \\ d \end{pmatrix} \right] \right\} \tag{5-3}$$

Index	Name	Building Description
0	Open	Exposed people without benefit of an overhead roof
1	Wood-Roof	Wood roof
2	Wood-1st	1st floor beneath roof of wood-framed structure
3	Wood-2nd	2nd floor beneath roof of wood-framed structure
4	Steel-Roof	Steel roof
5	Steel-1st	1st floor beneath steel roof structure
6	Steel-2nd	2nd floor beneath steel roof structure
7	Concrete-Roof	Reinforced concrete roof
8	Concrete-1st	1st floor beneath concrete roof
9	Concrete-2nd	2nd floor beneath concrete roof
10	Light-Metal	Roof of pre-engineered metal structure (or vehicle)
11	Composite	Layered roof made up of light-weight, non-metallic materials
12	Tile-Roof	Tile roof
13	Tile-1st	1st floor beneath tile roof of wood-framed structure
14	Tile-2nd	2nd floor beneath tile roof of wood-framed structure

Table 5-2. Roof Penetration Models.

a person would be seriously injured by a single impacting fragment. In the simplest case, this is the area of a person plus a region around the person to account for the size of the fragment. The casualty area calculation for people within structures must also consider the possibility that the fragment does not penetrate the roof of the structure (i.e., some probability of zero casualty area) and the possibility that when the fragment penetrates the roof, failure of roof elements causes additional debris to fall through increasing the effective casualty area. The casualty area can be less than the area of a person when averaged over all of the impacts of the particular fragment weight because the fragment may only occasionally be able to penetrate the roof and cause an injury. Note that the casualty area is basically zero for fragments that weigh less than one pound at impact with any of these roof types.

The figure depicts casualty areas as a function of fragment weights for six construction types. Both casualty area and

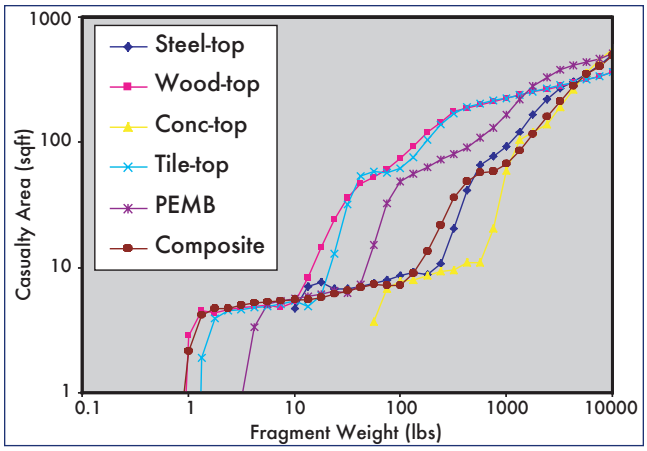

Figure 5-2. Example Casualty Areas for Steel Debris Impacting at Terminal Velocity.

fragment weight are plotted on a logarithmic scale. The "stair step" appearance results from multiple roof failure modes. The lowest "step", smallest fragment weight, results from fragments "punching through" the roof, generating little additional debris. The second "step" results from failures of joists causing a larger amount of roof structure to impact the floor below. The final "step" results from more massive structural failure in which the impacting fragment brings down substantial amounts of roof debris.

The figure illustrates the difficulty in answering the question of which roof provides the most protection without specifying the particular fragment characteristics. For fragments weighing up to a few thousand pounds, concrete offers the greatest amount of protection, followed by steel, pre-engineered metal (PEMB), tile, and finally wood. By contrast, for the more massive fragments, the order is altered because the impacting fragments cause partial or total roof collapse. The collateral damage of roof debris increases the casualty area according to the weight of the roof materials; concrete debris creates much larger casualty areas than the corresponding wood debris.

5.3 Data

The 2000 U.S. Census [11] provides a great wealth of data applicable to this study. It is complete (covers the entire area), detailed (small geographic regions), and has many data items that can be used to estimate sheltering. The Census "Summary File 3" (SF3) contains the demographic data useful for this work; and data is indexed by a unique table number (such as P31) and element number (such as P031001). There are several steps involved in making use of the data:

- Determining the demographic data items that will be useful for determining sheltering for homes, occupations, and/or schools, and the data used to calculating the percentages of people at school and at work.
- Developing translation tables (matrices **O** and **H** above) based on the demographic data items retrieved.
- Retrieving and geo-referencing all the necessary data.

This section details each of these topics.

5.3.1 Choosing Census Data Items

First, the choice of census data items must be made. There are many tables in the U.S. census, but for only a few is there a likely correlation with structure type. Based on a review of all the census tables, those most helpful to determine building distributions for people in different activities were selected. This section details which census tables were chosen, and how they are used to compute the values for sheltering. The tables which are used to translate from census category to structure type are discussed in the next section.

The census table "Units in Structure" (SF3, table H30) can be used to infer structure type for people at home. Building size is typically correlated with a structure type. For example, most single-family residences are wood frame buildings with wood or tile roofs. The data item "1 unit in structure" would correspond to a single-family residence. Likewise, large apartment complexes are likely to be multi-story structures. For the "50+ units in structure," most buildings have steel or concrete roofs and have many stories. The number of people at home is computed by subtracting the number of people at work and at school from the total population, and it can vary by scenario. The percentage of people who are outside while they are at home varies is assumed to be 20% for daytime on a weekend in the winter.

Estimating the total number of people at work is somewhat complicated. However, only a small percentage people are likely at work on a Saturday morning—2% of the working population is assumed for this study. Therefore, risk estimates are not very sensitive to the building distribution of people at work. A detailed algorithm was used to determine the allocation of working people to structure categories based on occupation [7], but is not described here. Similarly, only a small percentage of people are in school on a Saturday morning. In this study, 2% of the enrolled school population is assumed to be at school.

In addition, in the 2000 Census, there is a category of people in "Group Quarters" (SF3, table P9, item P009025). This population includes institutionalized and non-institutionalized people. For this study, these people tallied separately from people in other categories. They are always counted as being protected by the "group quarters" structure distribution (i.e. it is assumed they are never in an occupation or in school).

5.3.2 Translation to Building Types

Engineering judgment was applied in order to develop translations from demographic data to building distributions. Using their experience from looking at buildings and developing sheltering models, several experts independently estimated building distributions for each census category. In order to simplify the process, each expert chose several roof types and a height distribution for each roof type. These estimates were compared, and discrepancies discussed. The resulting translation from demographic data item to structure distribution is shown in Table 5-3 for people at home, Table 5-4 for people at work, and Table 5-5 for people at school

	Roof Type														
Census Category	1	2	3	4	5	6	7	8	9	10	11	12	13	14	Car
Group quarters	29.8	12.9	2.3	4.3	2.8	3.0	6.4	4.1	4.5			16.6	7.2	1.3	5.0
1-detached	57.0	3.0	0.0									28.5	1.5	0.0	10.0
1-attached	57.0	3.0	0.0									28.5	1.5	0.0	10.0
2 units	54.8	5.3	0.0									27.4	2.6	0.0	10.0
3 or 4 units	48.6	9.6	1.8									24.3	4.8	0.9	10.0
5 to 9 units	29.8	12.9	2.3	5.4	2.8	1.7	5.4	2.8	1.7			16.6	7.2	1.3	10.0
10 to 19 units	26.5	11.5	2.0	8.2	4.2	2.6	8.2	4.2	2.6			13.3	5.8	1.0	10.0
20 to 49 units	20.2	8.2	1.6	11.1	6.9	7.0	11.1	6.9	7.0			6.7	2.7	0.5	10.0
50 + units	12.6	6.6	0.8	7.3	6.7	15.9	9.2	7.5	13.3			6.3	3.3	0.4	10.0
Mobile home	42.8	2.3	0.0							45.0					10.0
Boat, RV, van, etc.	42.8	2.3	0.0							45.0					10.0

Table 5-3. Translation Table for Houses/Apartments

	Roof Type															
Census Category	0	1	2	3	4	5	6	7	8	9	10	11	12	13	14	Car
Management occupations, except farmers and farm managers		11.7	6.5	1.8	7.7	6.4	10.9	9.0	7.0	9.0		20.0	5.6	3.0	0.3	1.0
Farmers and farm managers		28.5	1.5	0.0							25.0	20.0				25.0
Business operations specialists		11.7	6.5	1.8	7.7	6.4	10.9	9.0	7.0	9.0		20.0	5.6	3.0	0.3	1.0
Financial specialists		11.7	6.5	1.8	7.7	6.4	10.9	9.0	7.0	9.0		20.0	5.6	3.0	0.3	1.0
Computer and mathematical occupations		11.7	6.5	1.8	7.7	6.4	10.9	9.0	7.0	9.0		20.0	5.6	3.0	0.3	1.0
Architects, surveyors, cartographers, and engineers		11.7	6.5	1.8	7.7	6.4	10.9	9.0	7.0	9.0		20.0	5.6	3.0	0.3	1.0
Drafters, engineering, and mapping technicians		11.7	6.5	1.8	7.7	6.4	10.9	9.0	7.0	9.0		20.0	5.6	3.0	0.3	1.0
Life, physical, and social science occupations		11.7	6.5	1.8	7.7	6.4	10.9	9.0	7.0	9.0		20.0	5.6	3.0	0.3	1.0
Community and social services occupations		11.7	6.5	1.8	7.7	6.4	10.9	9.0	7.0	9.0		20.0	5.6	3.0	0.3	1.0
Legal occupations		11.7	6.5	1.8	7.7	6.4	10.9	9.0	7.0	9.0		20.0	5.6	3.0	0.3	1.0
Education, training, and library occupations		20.9	5.3	3.8	16.3	8.4	5.2	16.3	8.4	5.2		5.0	2.7	1.2	0.2	1.0
Arts, design, entertainment, sports, and media occupations	20.0	17.7	2.4	0.0	8.7	7.0	9.3	8.7	7.0	9.3						10.0
Health diagnosing and treating practitioners and technical occupations		12.0	6.8	1.3	8.6	7.4	13.9	8.7	7.0	9.3		15.0	5.6	3.1	0.3	1.0
Health technologists and technicians		12.0	6.8	1.3	8.6	7.4	13.9	8.7	7.0	9.3		15.0	5.6	3.1	0.3	1.0
Healthcare support occupations		12.0	6.8	1.3	8.6	7.4	13.9	8.7	7.0	9.3		15.0	5.6	3.1	0.3	1.0
Fire fighting, prevention, and law enforcement workers, including supervisors	20.0	1.3	0.6	0.1	9.9	4.3	0.8	16.6	7.2	1.3		2.0	0.7	0.3	0.1	35.0
Other protective service workers, including supervisors	10.0	1.3	0.6	0.1	16.6	7.2	1.3	26.5	11.5	2.0		2.0	0.7	0.3	0.1	20.0
Food preparation and serving related occupations		34.6	4.2	0.2	8.5	5.5	6.0	8.5	5.5	6.0		5.0	13.2	1.7	0.1	1.0
Building and grounds cleaning and maintenance occupations	20.0	24.4	2.6	0.1	7.7	5.0	5.4	7.7	5.0	5.4		1.0	0.7	0.3	0.1	15.0
Personal care and service occupations		34.6	4.2	0.2	8.5	5.5	6.0	8.5	5.5	6.0		5.0	13.2	1.7	0.1	1.0
Sales and related occupations		33.8	5.0	0.2	7.6	5.6	6.9	7.6	5.6	6.9		5.0	12.9	2.0	0.1	1.0
Office and administrative support occupations		12.7	6.0	1.4	10.3	7.8	11.9	10.2	6.9	7.9		15.0	5.9	2.7	0.4	1.0
Farming, fishing, and forestry occupations	50.0	4.8	0.3	0.0	0.5	0.0	0.0	0.5	0.0	0.0	5.0	5.0	4.8	0.3	0.0	29.0
Supervisors, construction and extraction workers		12.7	6.0	1.4	10.3	7.8	11.9	10.2	6.9	7.9		15.0	5.9	2.7	0.4	1.0
Construction trades workers	40.0										20.0					40.0
Extraction workers	40.0										20.0					40.0
Installation, maintenance, and repair occupations	20.0	24.9	4.6	0.5	7.2	4.7	5.1	6.8	4.4	4.8		1.0	0.7	0.3	0.1	15.0
Production occupations		3.2	1.6	0.2	10.8	2.9	0.3	15.4	4.2	0.4	50.0	5.0	3.2	1.6	0.2	1.0
Supervisors, transportation and material moving workers	30.0										50.0					20.0
Aircraft and traffic control occupations	10.0				23.6	5.6	0.8	23.6	5.6	0.8						30.0
Motor vehicle operators	10.0															90.0
Rail, water and other transportation occupations	25.0										25.0					50.0
Material moving workers	33.3										33.4					33.3

Table 5-4. Translation Table for Occupations.

	Roof Type															
Census Category	0	1	2	3	4	5	6	7	8	9	10	11	12	13	14	Car
Group Quarters	varies	29.8	12.9	2.3	4.3	2.8	3.0	6.4	4.1	4.5			16.6	7.2	1.3	5.0
Schools	15.0	34.2	3.3	0.0	9.3	4.8	3.0	9.3	4.8	3.0	0.0	4.3	7.7	0.8	0.0	0.9

Table 5-5. Translation Table for Schools and Group Quarters

and in group quarters. These tables are used in Equation (5-2) to calculate the overall building distribution.

5.3.3 Retrieving and Correlating Data

Two other census elements are necessary: the geographic coordinates and the population counts. The census data is organized by records, with each record specifying some geographic area. The records are organized by summary level, which describes the type of geographic entity. For example, one summary level is "county" and another is "state". Each record can be correlated to a particular geographic region by matching the appropriate data fields with the attributes in the census cartographic boundary files for the correct summary level.

For a population model, it is important to choose the geographic region size appropriately. Once the regions are small compared to the debris dispersions, it is not cost-effective to choose smaller regions. In addition, there is inherent uncertainty in applying the census data, due to commuting, visitors, etc. The smallest geographic entity in the U.S. Census is the "block group", and a population model composed of all block groups is the highest resolution. However, block group size is based on population, so higher density regions (cities) have very small block groups. This is unnecessary detail for a risk analysis. A dual solution is used in this study. The "census designated places" (CDPs, with summary level=160) account for higher density locations, and these are also convenient because they correspond uniquely to named places. However, rural areas are not included within summary level 160 (since they are not CDPs). Outside of CDPs, block groups are used (level 090/091). These are selected by selecting only records with level 090/091 which have the field Place=99999, which indicates they are outside of a CDP. This solution offers a good balance between the number and size of population regions.

The census summary files include also the "GEO" table, which provides some data used to develop the population model. This includes an interior point (latitude/longitude, which is the approximate geographic center), a name, and the area (excluding water) for each geographic entity. While this data is also in the cartographic files, it requires more processing to extract, so therefore the data from the GEO table is used when creating the model. The GEO table also provides the total population for each entity (POP100) field, and this value is used to multiply by the sheltering percentages determined for each region (value p in Equation (5-2)).

5.4 Resulting Ground Exposure Model

The resulting population model with sheltering is shown in Figure 5-2, along with polygons to show the major debris regions. The blue region shows the main debris field where over 97% of all recovered debris was found. The green region shows a region where all credible Columbia debris was found—a few obvious erroneous coordinates have been excluded. The population map represents each population center as a square, with the size corresponding to the area of the population center, and the color the density of people in the region. Some population centers overlap others, as some census regions completely encircle others. Dallas/Ft. Worth can be easily seen just above the left edge of the blue region, and Houston is at the bottom center of the region.

The population model with sheltering includes all of the population and all of the area of Texas and Louisiana. It includes nearly 10,000 population centers, accounting for over 25 million people. The population is allocated to 16 sheltering categories in each population center. The average distribution of the population to the sheltering categories is shown in Table 5-6. A total of 18.7% of the people are in the open, and 70% are sheltered only by light structures (cars, wood/tile roofs, composite roofs).

Structure Type	Percentage	Structure Type	Percentage
Wood-Roof	39.9%	Concrete-Roof	1.5%
Wood-1st	3.1%	Concrete-1st	1.0%
Wood-2nd	0.3%	Concrete-2nd	1.1%
Steel-Roof	1.4%	Tile-Roof	18.1%
Steel-1st	0.9%	Tile-1st	1.5%
Steel-2nd	1.3%	Tile-2nd	0.1%
Light Metal	3.2%	Car	7.1%
Composite	0.8%	Open	18.7%

Table 5-6. Average Sheltering Distribution.

5.5 Aircraft Exposure Model

In order to determine the risks to aircraft, the probability of debris hitting a particular size aircraft at a particular speed must be calculated. Just as for population on the ground, the type of structure is important for determining risks. However, for aircraft, the strength is not the relevant parameter, because in this study, all parts of all aircraft are vulnerable to all potential debris. However, the probability of a debris impact with aircraft increases with aircraft size and with speed. Therefore, a large commercial aircraft (i.e. a Boeing 747) is the most likely to be impacted by debris. However, there are typically many fewer larger aircraft than small in any given

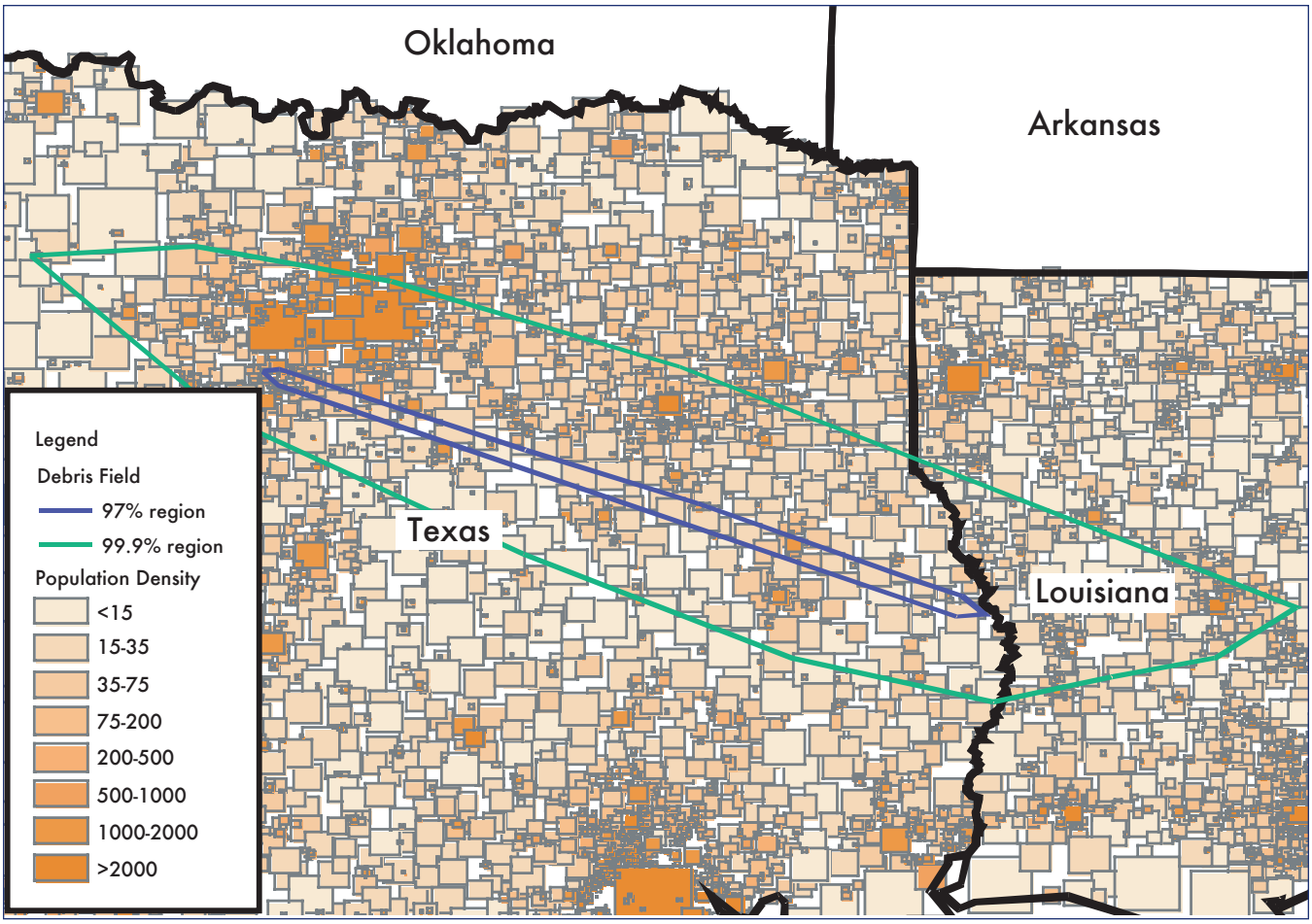

Figure 5-3. Population Model and Impact Area Defined by Recovered Debris.

region. Therefore, it is also instructive to determine the risks to a small private aircraft (such as a Cessna 172). The parameters used for the impact analyses with these two types of aircraft are shown in Table 5-7.

The density of aircraft is determined from the results of a previous study [7]. A complex procedure with data from all airports was used to determine density of aircraft in California as a function of location and altitude. For this study, it was assumed that the aircraft density in the debris field would be similar to the Central Valley of California. Like this region, the region of the debris field is relatively rural. Also, the Central Valley is near to a large metropolitan area (Los Angeles & San Francisco Bay Area), and the debris field is near to Dallas/Ft. Worth. For simplicity, the density of large planes was assumed to be the calculated density at 25,000 feet, while the density of small planes was assumed to be the density at 5,000 feet. The following table shows the density of the two types of planes in several ways.

	Boeing 747	*Cessna 172*
Altitude (feet)	38,000	7200
Speed (knots)	500	120
Front area (square feet)	480	52
Top area (square feet)	3000	281

Table 5-7. Aircraft Parameters for Impact Analysis.

	Boeing 747	*Cessna 172*
Areal density (planes per square nautical mile)	8×10^{-4}	3×10^{-2}
Average horizontal separation (nautical mile)	60	10
Volumetric density (planes per cubic nautical mile)	2×10^{-4}	1×10^{-2}

Table 5-8. Aircraft Density.

6. Risk Analysis Due To Columbia Debris

6.1 General Procedure

The risk analysis process in CRTF evaluates each footprint for each debris category and each initial state vector and computes a probability of impact in each of the population centers in the population library. The impact probability on a population center is computed based on a bivariate normal distribution and represents the volume over the area of the

population center. This is demonstrated in Figure 6-1. The methods used by CRFT to estimate bivariate normal impact probability distributions are described in Appendix A.

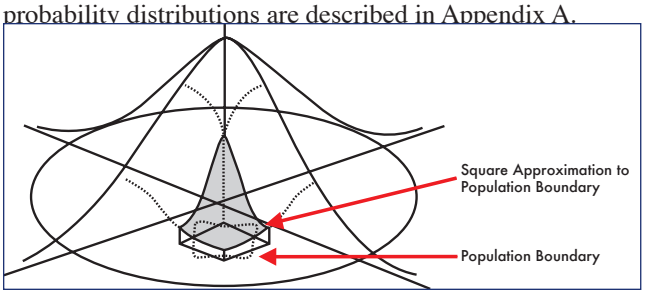

Figure 6-1. Integration of the Bivariate Normal Debris Impact Distribution Over the Area of the Population Center to Determine the Probability of Impact Upon the Population Center.

The equation for casualty expectation, given an initial state vector for debris group "i" that could impact on population center "j" is

$$E_{Cij} = P_{Iij} A_{Ci} N_{Fi} \frac{N_{Pj}}{A_{Pj}} \quad (6\text{-}1)$$

Where P_{Iij} is the impact probability of debris group "i" in that particular class (ballistic coefficient and state vector) on population center "j", A_{Ci} is the casualty area for that fragment class "i" on that population center considering whether the person is outside or sheltered and in what shelter category, N_{Fi} is the number of fragments in that category, N_{Pj} is the number of people in population center "j" and A_{Pj} is the area of the population center. (Note this equation is simplified, since in general there may be another summation over various shelter categories, since each fragment group may have a different casualty area for each shelter category.)

To obtain the total casualty expectation, sum over all cases of fragments classes "i" and population centers "j", i. e.

$$E_{C-Total} = \sum_i \sum_j E_{Cij} \quad (6\text{-}2)$$

If the $E_{C\text{-}Total}$ computed in this study is greater than 0.5, then a casualty would be the expected consequence. If it is less than 0.5, then casualties are not the expected consequence of a single event, but casualties are still possible.

6.2 Computed Risks Using the Breakup Model, the Casualty Model and CRTF/RRAT

Table 6-1 summarizes the risks from the model developed using the gathered and processed fragments. The population model for the day and time of day assumes that 18% of the people are outdoors and 82% are inside with various levels of sheltering. The four groups identified in the table are from the groupings identified in Section 2. Note that Group 1 totally dominates the risk and the effects of the two streaks identified as Groups 2 and 3 and the scatter identified as Group 4 are totally inconsequential. If we assume that there is no other debris that survived, then the model indicates that the total casualty expectation is 0.111 (considering sheltering) which is a number less than 0.5. Therefore, the lack of seriously injured people on the ground was the most likely (i.e. expected) result of this accident.

	Number of Fragments	Weight (lb)	Ec
Group 1	73319	82287	0.11
Group 2	537	942	0.0002
Group 3	316	1239	0.0003
Group 4	540	1801	0.0003
Total	74712	86269	0.111

Table 6-1. Ground Risk Results Based on Gathered Debris (Model).

If we assume that the Columbia broke up, but all fragments survived, and assume the recovered debris is representative of the "un-recovered debris," then the E_C due to all debris surviving is 0.29. These assumptions are considered quite conservative because (1) it is almost certain that some debris burned up during re-entry, and (2) much of the un-recovered debris is likely to be smaller than the recovered fragments, and thus not potentially casualty producing. Table 6-2 shows that the E_C ranging from recovered debris, to 60, 80 and 100% surviving. Table 6-2 also contains the probability that there will be one or more casualties.

Debris Case	Percentage of total Orbiter/ Payload weight	E_C - Sheltered	P [≥ 1 casualty]
Model (recovered debris)	38%	0.14	0.13
60% of total wt. survived	60%	0.21	0.19
80% of total wt. survived	80%	0.29	0.25
100% of total wt. survived	100%	0.36	0.30

Table 6-2. Ground Risk Results as a Function of Amount of Debris Assumed to Survive.

Figure 6-2 shows the risk profile, P(≥ n casualties) as a function of n, for each of the debris cases.

Individual risk was also computed. Looking at the case where only recovered debris is considered, the highest

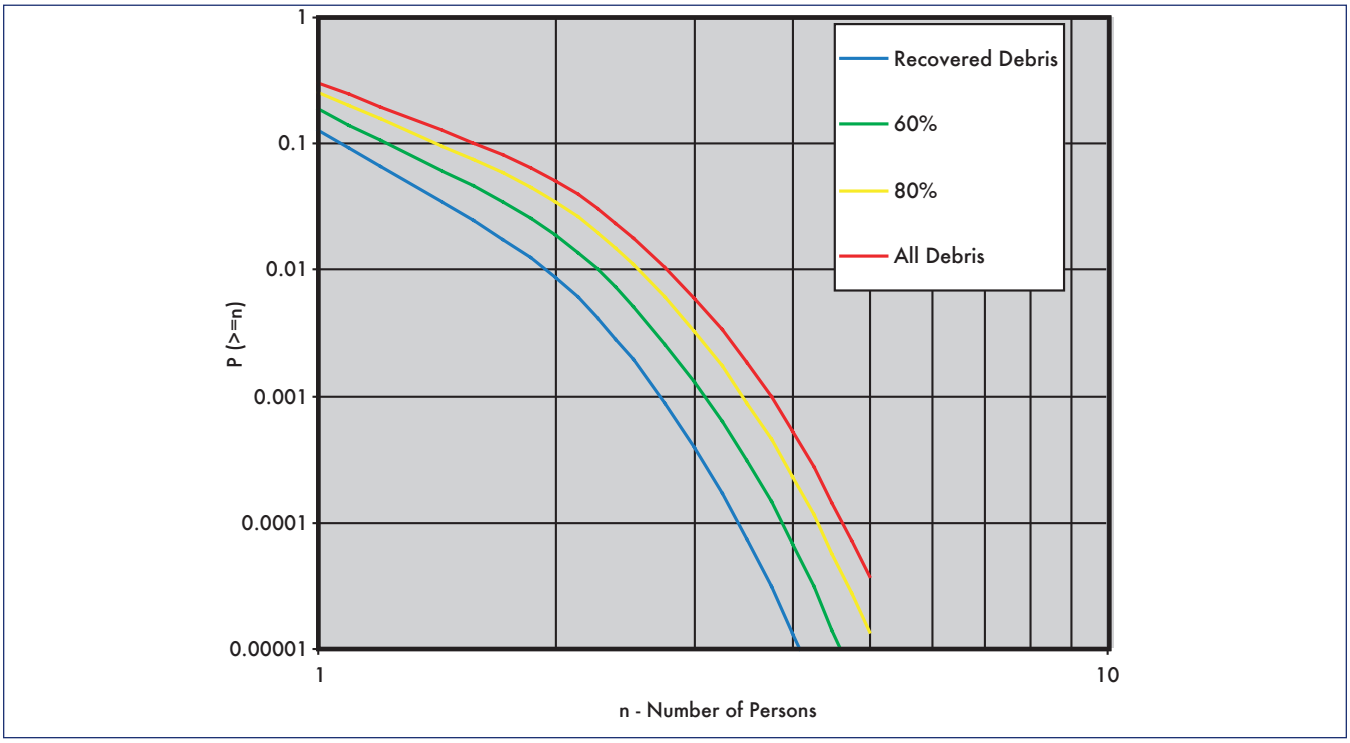

Figure 6-2. Debris Risk Profiles for Different Percentages of Surviving Debris.

computed risk to any individual exposed to the debris field was determined to be 7.6×10^{-5}. The number increased proportionately for those cases where more debris was assumed to survive. The largest number after examining all the population centers was the largest individual E_C. Since the E_C for one person is equivalent to the probability of the person becoming a casualty, the statement in terms of probability is "the highest probability of any particular person exposed to the recovered debris becoming a casualty was 7.6×10^{-5}."

6.3 Risk to Aircraft

The collision between two moving bodies depends on the velocities and dimensions of the two bodies. We define the velocity of the aircraft as $\mathbf{v}_a$, the velocity of the debris as $\mathbf{v}_d$, the characteristic length of the debris as x_d, and the length, width, and height of the airplane as l, w, and h, respectively. It is useful to define the angle φ as the orientation of the relative velocity vector of the debris and aircraft with respect to the local vertical. This angle is given by

$$\varphi = \tan^{-1}\frac{|\mathbf{v}_a|}{|\mathbf{v}_d|}$$

For simplicity, it is assumed that the debris falls vertically and the aircraft flies horizontally. This is a good approximation for the Columbia accident; except for a few fragments with large ballistic coefficients, the horizontal velocity component is relatively small by the time the debris reaches altitudes where aircraft may be present.

For a single aircraft, the volume in which a collision occurs is the volume of space swept out by the aircraft in the time

$$t_{fall} = \frac{x_d + h}{|\mathbf{v}_d|}$$

it takes the debris to fall the height of the aircraft. The time of the fall is

The volume swept out by the aircraft must be determined from area of the aircraft as viewed from the fragment. An area of collision for plan view is

$$A_{PLAN} = (l + x_d)(w + x_d)$$

The front area of collision is

$$A_{FRONT} = (w + x_d)(h + x_d)$$

For an airplane, which is not a simple box, the plan and front areas can be defined more carefully based on the actual areas of the airplane. The area of the aircraft from the perspective of the debris is

$$A_{sweep} = A_{FRONT}\cos\varphi + A_{PLAN}\sin\varphi.$$

The collision volume is the volume of the airplane plus the volume swept out by the aircraft moving for time t_{fall},

$$V_{collision} = l\,w\,h + A_{sweep}\,|\mathbf{v}_a|\,t_{fall}\,.$$

The probability of debris impacting a single hypothetical airplane assumed to fly through a particular space at a given time is the collision volume multiplied by the probability density of debris at that point:

$P_I = (x,y,z) = V_{collision} d_{debris}(x,y,z)$.

CRTF can compute the density of fragments as a function of time and position while the debris is descending. It uses trivariate normal distributions to model dispersions about the nominal descent trajectory for each fragment group originating from each state vector. CRTF computes the characteristics of each distribution from release to impact at small time steps. These 3-dimensional distributions are used to compute $d_{debris}(x,y,z,t)$ in the aircraft risk computation.

The probability density of debris was calculated by CRTF from the sum of all the distributions of debris from each breakup time. By calculating the probability of impact with airplanes for many combinations of breakup times and aircraft different positions and altitudes, $P_I(x,y,z)$ can be determined for each type of airplane.

The plot of impact probability density has a similar shape for all classes of airplanes at all altitudes; only the magnitude of the impact probability density varies. This plot is visually indistinguishable, except in absolute magnitude, with a probability of impact chart on the ground.

The worst case probability of a debris impact on any single plane can be determined by finding the maximum $P_I(x,y,z)$ from the breakup analysis. For a commercial aircraft, the worst case was 0.08, and for general aviation for a single plane, it was 0.0037.

For each class of aircraft, the expected number of impacts with debris per mission, E_I, can be calculated by integrating over all space the probability of impact multiplied by the density of airplanes, as

$$E_I^j = \iiint_{all\ space} E_{3D}^j(x,y,z) P_I^j(x,y,x)\, dx\, dy\, dz$$

$$E_I^{total} = \sum_{j=1}^{N_{classes}} E_I^j$$

where j is the airplane class. For this study, the density of planes is assumed to be a constant for each airplane class, as discussed in the previous section on the aircraft exposure model. The total E_I for a trajectory is the sum of the E_I's of each airplane class,

The expected number of planes impacted by the Columbia breakup was approximately 3×10^{-2}. This is primarily due to possible impacts with general aviation (>80%).

6.4 Validation of Computed Risks Using a Simplified Model

This section compares the CRTF computed risks with an alternate simplified model that assumed the exposed population had a uniform density and that only people without shelter are vulnerable to serious injuries due to *Columbia* debris impacts. The average population density over the region at risk was approximately 85 people / per square nautical mile. The total casualty area for people in the open was determined in Section 4 and presented in Table 5-2. Table 5-6 presented an estimate of the percentage of people without shelter. The product of these three values are given in Table 6-3 along with the results from the CRTF analysis that accounted for the potential casualties indoors as well as the distributions of population and debris impacts. Since Table 5-2 also contains hazard and fatality areas, these can also be used in estimating the expected hazard and the expected number of fatalities. These results are also included in Table 6-3.

The results of the simplified analysis in Table 6-3 give an estimate of the casualty expectation that is 60% of the values in the detailed analysis. Since the approximate analysis is quite intuitive, these results provide support to the results from the detailed analysis. The fact that the detailed analysis produced higher risk estimates than the simplified analysis also suggests that the population density was also relatively high where the debris impact density was also relatively high. Examination of Figures 3-7 and 5-3 indicates that, indeed this appears to be the case. Furthermore, the debris recovery effort seemed to show that Nacogdoches, TX, which was the most significant concentrated population center in the vicinity of the debris impacts, was in an area of relatively high debris impact density. This result may be influenced by the fact that more debris is likely to be seen and recovered in highly populated areas compared to areas away from roads, buildings, and tended property. However, ACTA found no statistically significant correlation between the location of recovered debris and population density.

The E_{Haz} in Table 6-3 includes all of those cases where debris can hit someone and not result in an injury. A large number of the collected Columbia fragments are in this category. The E_{Haz} in Table 6-3 is typically five times the E_C. In addition,

Debris Case	Percentage of Total Orbiter and Payload Weight	E_{Haz}	E_C	E_F
Model (gathered debris)	38%	0.41	0.08 (0.14)	0.06
60% of total wt. survived	60%	0.66	0.13 (0.21)	0.10
80% of total wt. survived	80%	0.88	0.18 (0.29)	0.13
100% of total wt. survived	100%	1.11	0.22 (0.36)	0.16

Note: All results based on the assumption of a ground wind of 10 ft/s and a population density of 85 people/per square nautical mile).
Numbers in parentheses represent the numbers computed in the detailed analysis.

Table 6-3. E_{Haz}, E_C and E_F from the Approximate Analysis.

the ratios between the E_C's and the E_f's indicate that 75% of the casualties will be fatalities. Note that the absolute values of the numbers in the table are considered less accurate than those from the detailed analysis, but the relative values in the table are considered quite representative.

6.5 Sensitivity of Results to Model Parameters

A formal uncertainty analysis was not performed due to the limited time available for this study. However, sensitivity studies were performed to determine the sensitivity of the computed risks to the following critical model parameters.

1) Sensitivity to the amount of debris that survives reentry to impact the ground.

   The computed risk to the public shifts up and down directly proportional to the percentage of the debris that survives. This was demonstrated in Table 6-2:

2) Sensitivity to the assignment of numbers of fragments to each ballistic coefficient group.

   The model, based on the recovered fragment data, has a large number of fragments with low ballistic coefficients. One test of the stability of the answer is to shift the numbers of fragments to cells with higher ballistic coefficient to see if higher numbers of fragments in the higher ballistic coefficient cells would increase the risk. This test was accomplished in two steps:

   a) All of the fragment counts were shifted one ballistic coefficient category, i.e. fragments that were in the β=0.5 category were shifted to β=1.0 category, β=1.0 to the β=1.78 category, etc. Compute the total E_C using the approximate method in Section 6.4 and compare with the E_C for the unshifted case.

   b) Repeat the Step 1 process by shifting all of the fragment counts one more ballistic coefficient category. Again, compute the E_C and compare with the unshifted case.

      The results of this exercise indicate an increase of E_C of 50% for a one-cell shift of fragment count and 125% for a two-cell shift of fragment count. However, each higher β cell also has a higher average fragment weight. If the total fragment count is adjusted downward after the shift, to maintain the total fragment weight, the risk actually decreases by about 29% for a one-cell shift and 53% for a two-cell shift.

      This latter test is not really valid because the total number of fragments cannot be decreased from the actual gathered count. However, the important result from this test is that shifts in the cells will not make major shifts (i.e. order of magnitude) in the final result.

3) Sensitivity to a shift in the initial breakup point of the Orbiter.

   One test was made where the breakup point was shifted to 50 seconds earlier, moving the footprint approximately 100 nm uprange along the reentry path. The breakup state vectors were recomputed for this condition and the risk analysis was performed again using these state vectors. The result, in this case, was an increase in the calculated risk to the public by about 36%. The increased population density south of Dallas was responsible for the increased risk.

4) Sensitivity of the public risk to a shift in the assumption of 20% of the people at home at 8:00AM on Saturday morning being outside.

% Debris Surviving	*People at home 10% in the open*	*People at home 20% in the open*	*People at home 30% in the open*
Model – 38% of total wt.	0.08	0.14	0.21
60% of total wt. survived	0.11	0.21	0.32
80% of total wt. survived	0.15	0.29	0.44
100% of total wt. survived	0.18	0.36	0.54

Table 6-4. Sensitivity of the Final E_C Results to the Assumption of the Percentage of the People at Home who are Outside.

   The public risk was computed using CRFT for 30% of the people at home being outside and 10% of the people at home being outside. The results are presented in Table 6-4.

   The results in Table 6.4 shows that the public risk estimate given the Columbia accident is linearly related to the percentage of people without sheltering. This result indicates that public risk from the Columbia accident would have been substantially mitigated by landing during the middle of the night, when almost everyone is inside a shelter and few aircraft are in flight.

5) Sensitivity of the public risk due to shift of orbit such that the debris field falls over Houston.

   The risk, in terms of E_C, is increased by a factor of 10.5. The higher E_C and probability of casualty are due to the debris field lying over Houston. Houston is a little closer to the landing point of the Shuttle at KSC and thus lines up under the debris pattern when the orbit is shifted. The actual debris field from *Columbia* missed most of Dallas and fell in an area of much

lower population density.

For this case, the probability of one or more casualties is increased from a range of 0.13 to 0.30 For the actual *Columbia* debris impact to a range of 0.89 to 0.98 for the same debris field falling over Houston.

7. Study Conclusions And Recommendations

The following are the conclusions and recommendations for this study.

1) The results of the risk analysis indicate that the lack of casualties was the expected event, but there was a reasonable probability (less than 0.5 but greater than 0.05) that casualties could have occurred.

2) A preliminary evaluation of aircraft risk indicates that there was a lower likelihood of debris impact on commercial or general aviation aircraft than impact on people on the ground. However, the estimated probability of aircraft hit levels were higher than would be allowed for unrestricted aircraft operations.

3) Detailed fragment data were not available for the study (the details had not been developed yet) and therefore some engineering judgment was necessary to develop models of individual weights, dimensions, aerodynamic characteristics and conditions of impact. This lack of information increases the uncertainty in the accuracy of the final results. The study should be revisited after the fragment data has been fully processed.

4) A more detailed aircraft risk analysis should be performed using the actual records of aircraft activity at the time of the accident. This additional study should also take into consideration the vulnerability of the aircraft.

5) The risk to people on the ground due to the Columbia accident was predominately due to people in the open. To the extent that future Orbiter re-entry accidents are likely to produce similar debris impacts, public risk from Shuttle re-entry may be mitigated by landing during the middle of the night, when almost everyone is inside a shelter and few aircraft are in flight.

References

[1] Carbon, S., Common Real-Time Debris Footprint, Program CRTF7 User's Manuel, ACTA Report No. 01-451/23.1-01, Sept 2001

[2] Haber, Jerold M., Liquin Cao and John O. Morris, "Range Risk Analysis Tool (RRAT)," *Proceedings of the JANNAF 30th Propellant Development and Characteristics Subcommittee and 19th Safety and Environmental Protection Subcommittee Joint Meeting*, Colorado Springs, Colorado, March 2003

[3] Code of Federal Regulations (CFR) 14 CFR Part 415 Launch License, Federal Register / Vol. 64, No. 76 / April 21, 1999 /

[4] Range Commanders Council Standard 321-02, Common Risk Criteria for National Test Ranges, published by the Secretariat of the RCC US Army White Sands Missile Range, NM 88002-5110, June 2002

[5] Orbiter Thermal Protection System, NASA Facts, FS-2000-06-29-KSC, March 1997

[6] Salguero, D., Trajectory Analysis and Optimization Software (TAOS), Sandia National Laboratories, SAND99-0811, June 2001

[7] Larson, Erik and Jerold M. Haber. Final Quantitative Risk Analysis for Generic Lifting Entry Vehicle Landing at Edwards Air Force Base. Report No 01-474-04, ACTA Inc., Torrance, CA, October 2001. Also available from http://www.ealev.com/pdf/QRA.pdf.

[8] Hasselman, Timothy K., Mark R. Legg, and Mark C. Anderson. Casualty and Fatality Risk Models for Roof Penetration by Inert Debris. Technical Report 99-400/11.4-03, ACTA Inc., Torrance CA, September 1999

[9] Hasselman, Timothy K. and Mark R. Legg. Update of Casualty and Fatality Risk Models for Roof Penetration by Inert Debris. Technical Report 00-430/16.4-02, ACTA Inc., Torrance CA, September 2000

[10] Larson, Erik, and Jon Chrostowski. *Population Library with Sheltering for Overflight of Europe and the Middle East*. Report No. 02-481/4-04, ACTA Inc., Torrance, CA, September 2002

[11] United States Census Bureau. *2000 Census*. http://www.census.gov/main/www/cen2000.html

Appendix A

Reprint of Paper Describing CRTF[4]

Real-Time Debris Footprint

Steven L. Carbon and Jon D. Collins
ACTA, Inc.
2790 Skypark Drive Suite 310
Torrance, CA 90505

Abstract

During the launch of a rocket, range safety typically has used the track/locus of the vacuum instantaneous impact point (VIIP) as the indicator of vehicle position. When this track crosses pre-established abort lines, the Mission Flight Control Officer (MFCO) issues a command to abort the launch. The problem with the use of the IIP is that it does not actually show where the debris will impact. Thus decisions to abort are not based on a realistic depiction of the consequences, but rather the crossing of a point and a line, where the position of the line is adjusted to protect the public. There are situations where a more accurate display of the instantaneous debris impact dispersion will permit the MFCO more latitude. This is particularly important with manned launches such as the Space Shuttle and, in fact, a debris footprint has been used by the safety office at the Eastern Range to control the launch for some time.

This paper describes a new footprint program, CRTF (Common Real-Time Footprint) that was developed under the joint sponsorship of the Eastern and Western Ranges. The footprint differs in that it is probabilistically based and develops all of the dispersion data in real-time so that it can use the actual state vector as the starting point for the dispersion analysis. The resulting footprint can provide a statistical basis for the MFCO decision. Instead of an abort line, an Impact Limit Line (ILL) can be used for the abort decision, with probabilistic statements such as "99% sure that no fragment will land on the opposite side of the Impact Limit line if abort is initiated when the footprint touches the Impact Limit Line." The program is designed to compute very quickly and, as part of the RSA real-time system, it will update ten times/second.

The method uses a series of bi-variate normal distributions, with each representing the impact distribution for a different debris category. These distributions provide the basis of the probabilistic model. These same bi-variate normal distributions are also used in a risk model in the program to compute risk in real-time. CRTF also has a number of other features that can be used for various vehicle and tracking system failure modes.

Program Overview

CRTF is designed to compute the dispersions that define an instantaneous scenario of a vehicle breakup and dispersion of debris. It can be used in real-time to show instantaneously the statistical dispersion of debris impacts if the vehicle is destroyed at that instant, or it can be used as a subroutine in a risk analysis program that generates a large number of state vectors describing all of the potential accident/failure conditions along with their corresponding probabilities. Most of the dispersion models in CRTF originated in the LARA launch risk analysis program,[5] but their implementation is somewhat different in several cases because of the need to make the program run very fast in real-time.

The two most dominant effects on footprint length and shape are ballistic coefficient of the debris and the wind. The debris with very low ballistic coefficient decelerates very quickly and if the wind is light, it falls to the ground close to the sub-missile point at the time of breakup. If the wind is strong, the debris will move with the wind and land in the direction of the wind relative to the breakup point. If the debris has a very high ballistic coefficient, it moves with little effect of the wind and lands in the direction of the vacuum impact point. Figure 1 illustrates the effects of ballistic coefficient and wind on the "centerline" of debris footprint.

The dispersion relative to the debris centerline is the result of impulses and uncertainties from a number of sources. These are illustrated in Figure 2. The "disks" around the impact points in Figure 2 represent the impact uncertainty of debris due to the uncertainty sources. Four pieces of debris are shown, but actually there can be thousands. To simplify the modeling process, debris pieces are grouped into classes. There may be 50 or more classes, each containing debris

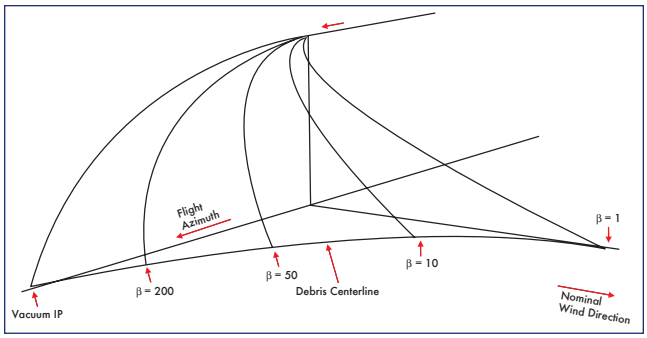

Figure 1. The influence of the ballistic coefficient.

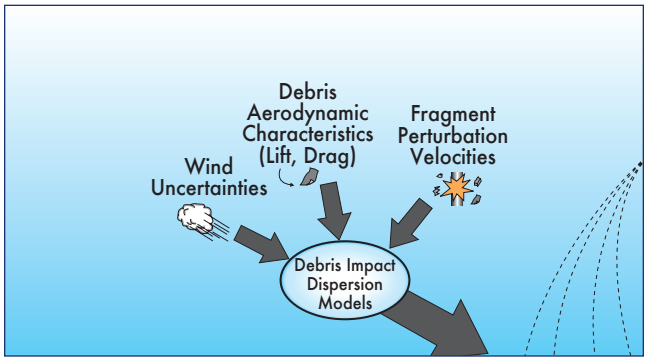

Figure 2. Contributions to debris dispersion models.

pieces that have similar ballistic coefficients, explosive characteristics or velocity perturbation characteristics. The CRTF process is to simulate the behavior and impact dispersions of each of these groups and then, in the final step, adjust the statistical results to account for the number of fragments in the group.

CRTF was designed to operate in real-time with an update rate of 10 times per second. Another specification of the program was that it must operate off the actual state vector and no tables were permitted that were developed before launch and used in a look-up mode. Previous programs developed for the Western and Eastern Ranges used look up tables based on vehicle altitude or velocity at the time of destruct. This requirement was difficult but became workable as the capability of computers improved. The speed requirement required considerable innovation in the program design. The impact predictor, for example, could not use a typical Runge Kutta algorithm, but had to use a faster three and a half order Taylor series concept (non-corrective) that, after adjustment, proved to be quite accurate.

CRTF contains a set of models that estimate the range of free-fall and impact locations of the fragments that result from vehicle breakup. The initiating event is assumed to be the activation of on-board destruct charges due to a command destruct signal, leading to total vehicle destruction into a fixed set of fragments. There are other breakup conditions (e.g. aerodynamic) but the intent of the program is to provide the impact dispersions if there is a destruct, thus providing the Mission Flight Control Officer with the probabilistic extent of the debris resulting from destruct action. The CRTF models attempt to quantify the uncertainties that exist in the

vehicle location at the moment of breakup, in the characteristics of the generated fragment debris, and in the external conditions during fragment free-fall. There are six uncertainty models in CRTF, four of which employ a Monte Carlo technique. The Monte Carlo routines are used to handle some of the uncertainties and develop impact distributions that contribute to the total uncertainty. The other impact uncertainties are developed using linear equations and covariance propagation, thus the program is a hybrid, taking advantages of the best of both statistical modeling methods.

Through judicious choice of input, one can isolate the execution of each individual uncertainty model. In the following paragraphs, each of the models is described.

(1) The real-time vehicle state vector, passed to CRTF, is generated from an estimation routine (Kalman filter) that utilizes tracking data from one or more sources. Each individual data source contains measurement error, which is implicit in the composite filter solution and is represented by the filter's covariance matrix.

$$\Sigma\,(x,y,z,\dot{x},\dot{y},\dot{z}) = \begin{bmatrix} \sigma_x^2 & \rho_{xy}\sigma_x\sigma_y & \rho_{xz}\sigma_x\sigma_z & \rho_{x\dot{x}}\sigma_x\sigma_{\dot{x}} & \rho_{x\dot{y}}\sigma_x\sigma_{\dot{y}} & \rho_{x\dot{z}}\sigma_x\sigma_{\dot{z}} \\ \rho_{yx}\sigma_y\sigma_x & \sigma_y^2 & \rho_{yz}\sigma_y\sigma_z & \rho_{y\dot{x}}\sigma_y\sigma_{\dot{x}} & \rho_{y\dot{y}}\sigma_y\sigma_{\dot{y}} & \rho_{y\dot{z}}\sigma_y\sigma_{\dot{z}} \\ \rho_{zx}\sigma_z\sigma_x & \rho_{zy}\sigma_z\sigma_y & \sigma_z^2 & \rho_{z\dot{x}}\sigma_z\sigma_{\dot{x}} & \rho_{z\dot{y}}\sigma_z\sigma_{\dot{y}} & \rho_{z\dot{z}}\sigma_z\sigma_{\dot{z}} \\ \rho_{\dot{x}x}\sigma_{\dot{x}}\sigma_x & \rho_{\dot{x}y}\sigma_{\dot{x}}\sigma_y & \rho_{\dot{x}z}\sigma_{\dot{x}}\sigma_z & \sigma_{\dot{x}}^2 & \rho_{\dot{x}\dot{y}}\sigma_{\dot{x}}\sigma_{\dot{y}} & \rho_{\dot{x}\dot{z}}\sigma_{\dot{x}}\sigma_{\dot{z}} \\ \rho_{\dot{y}x}\sigma_{\dot{y}}\sigma_x & \rho_{\dot{y}y}\sigma_{\dot{y}}\sigma_y & \rho_{\dot{y}z}\sigma_{\dot{y}}\sigma_z & \rho_{\dot{y}\dot{x}}\sigma_{\dot{y}}\sigma_{\dot{x}} & \sigma_{\dot{y}}^2 & \rho_{\dot{y}\dot{z}}\sigma_{\dot{y}}\sigma_{\dot{z}} \\ \rho_{\dot{z}x}\sigma_{\dot{z}}\sigma_x & \rho_{\dot{z}y}\sigma_{\dot{z}}\sigma_y & \rho_{\dot{z}z}\sigma_{\dot{z}}\sigma_z & \rho_{\dot{z}\dot{x}}\sigma_{\dot{z}}\sigma_{\dot{x}} & \rho_{\dot{z}\dot{y}}\sigma_{\dot{z}}\sigma_{\dot{y}} & \sigma_{\dot{z}}^2 \end{bmatrix}$$

This matrix contains both position and velocity uncertainty along each of three orthogonal axes. The model in CRTF assumes a normal distribution in each direction, and generates Monte Carlo samples for each of the six degrees of freedom.

where σ_x is the standard deviation of x, σ_y is the standard deviation of y, etc. and ρ_{xy} is the correlation coefficient of between the two variables, x and y. The x, y, z coordinate system is Cartesian in whatever frame used by the real-time system.

(2) There is a time delay between the moment of decision to send command destruct, and the time at which the charges on the vehicle respond. During this time delay, which is typically between three and five seconds, the vehicle may experience a failure and start to tumble or deviate from its trajectory. This course change is computed using malfunction tumble turn curves supplied by the vehicle's manufacturer. At each state time, there is a range of possible tumble rates depending upon the degree of offset of the thrust vector. The offset is due to a nozzle deflection or engine burn-through. Since the vehicle manufacturer is required to provide a series of tumble turn curves (velocity perturbation from nominal velocity and perturbed direction in velocity) for discrete engine offsets, these curves are considered as the discrete possibilities for a tumble turn (in any direction relative to the state vector). Each of these discrete thrust offsets is assigned a relative probability. Currently, in most applications, the program treats each of the tumble turns as equally likely, but the capability is there to vary the probability of each offset if the data is available from the manufacturer. Thus the program randomly selects the turn curve, randomly selects the direction away from the velocity vector and randomly selects the delay time before destruct.

(3) When fragments are produced at breakup, they are given an impulse away from the main explosion. This leads to both an imparted speed and direction for each fragment. Since the orientation of the vehicle is not known to the estimation generator, no preferred direction can be assigned to the fragments. Further, the fragment data input to CRTF only contains the maximum explosion speed that each fragment category may expect. To handle this explosion velocity uncertainty the CRTF model assumes that, along each of the three orthogonal axes, the speed obeys a normal distribution with a standard deviation given by one-third the maximum explosion speed. The full three-dimensional velocity then fits a Maxwellian distribution. Monte Carlo samples are obtained for each of the three speed components and are used to augment the state velocity.

(4) The size and shape of each fragment determines the drag effect during free-fall. The parameter that quantifies this atmospheric influence is the ballistic coefficient of the fragment. Due to the uncertain nature of the breakup of the vehicle, each fragment can only be assigned a range of ballistic coefficients. The values in this span are taken to obey a Gaussian distribution (it can be different, e.g. lognormal, triangular, etc.), where the two extremes and nominal value are specified by input to CRTF. The ballistic coefficient uncertainty model in CRTF generates Monte Carlo samples for each fragment category just prior to initiating the free-fall propagator. The ballistic coefficient may change during free-fall if the fragment contains burning propellant.

(5) During free-fall, the fragments experience a lift effect where the piece is subjected to a force perpendicular to its direction of motion. The lift force is largest for flat plates (as an aircraft wing), and at lower altitudes where the air density is greatest. The magnitude of the lift force fluctuates as the fragment tumbles since the surface along the direction of motion changes. The lift model in CRTF computes two impact points, starting from the initial state position. One location is for a fragment that sees no lift, and the second for a fragment that is given a constant lift. The lift is computed using a lift-to-drag coefficient that relates the relative effect compared to drag, and which is specified in the CRTF input for each fragment category.

(6) An external source of uncertainty applied to each fragment during free-fall is the strength of the wind. Several hours prior to vehicle launch, empirical wind measurements are obtained. The accuracy of these wind measurements decreases as the time since data acquisition increases. CRTF handles the aging wind

data, not by adjusting the wind used in the fragment propagator, but by computing separate wind uncertainty impact dispersions. The input to this calculation uses uncertainty data acquired over a period of years, which quantifies how much the wind speed and direction are in error for a given age of wind, a given season, and a given altitude. A wind covariance matrix is shown below. The wind dispersion effect is determined by computing the time a fragment traveling at terminal velocity passes through an altitude band and, assuming that the fragment is embedded in the wind, the fragment while falling through the band moves laterally at the velocity of the wind. This assumption is

$$\Sigma_{\text{Wind}} = \left[\begin{array}{cccc|cccc} \sigma^2_{E_1} & \sigma_{E_1E_2} & \cdots & \sigma_{E_1E_n} & \sigma_{E_1N_1} & \sigma_{E_1N_2} & \cdots & \sigma_{E_1N_n} \\ \sigma_{E_2E_1} & \sigma^2_{E_2} & \cdots & \sigma_{E_2E_n} & \sigma_{E_2N_1} & \sigma_{E_2N_2} & \cdots & \sigma_{E_2N_n} \\ \cdots & \cdots & \cdots & \cdots & \cdots & \cdots & \cdots & \cdots \\ \sigma_{E_nE_1} & \sigma_{E_nE_2} & \cdots & \sigma^2_{E_n} & \sigma_{E_nN_1} & \sigma_{E_nN_2} & \cdots & \sigma_{E_nN_n} \\ \hline \sigma_{N_1E_1} & \sigma_{N_1E_2} & \cdots & \sigma_{N_1E_n} & \sigma^2_{N} & \sigma^2_{N_2} & \cdots & \sigma_{N_1N_n} \\ \sigma_{N_2E_1} & \sigma_{N_2E_2} & \cdots & \sigma_{N_2E_n} & \sigma_{N_2N_1} & \sigma_{N_2N_1} & \cdots & \sigma_{N_2N_n} \\ \cdots & \cdots & \cdots & \cdots & \cdots & \cdots & \cdots & \cdots \\ \sigma_{N_nE_1} & \cdots & \cdots & \sigma_{N_nE_n} & \sigma_{N_nN_1} & \sigma_{N_nN_2} & \cdots & \sigma^2_{N_n} \end{array}\right]$$

$$\left[\Sigma^{\text{EN}}_{\text{Wind}}\right]_h = ????????????????????????????????$$

quite accurate for low ballistic coefficient debris (β=1 to 10 psf) and less so as β increases. Fortunately, the effect of ballistic coefficient on drift decreases as $1/\sqrt{\beta}$. The wind covariance matrix and the matrix product to obtain impact dispersions due to wind. Note, $\sigma_{EiEj} \equiv \rho_{EiEj}\,\sigma_{Ei}\,\sigma_{Ej}$, = etc.

For each active fragment group, the above six sources of uncertainty are combined by building three impact covariance matrices as follows. A set of N Monte Carlo simulations are set up to represent selections of random conditions. The number of simulations is specified by the user, and for real-time, N should be at least 100 cycles. For each simulation, CRTF determines the post-malfunction tumble turn position and velocity state vector and adds in the measurement error vectors and explosion velocity vectors. Next, the ballistic coefficient of the fragment group is sampled. The fragment is then propagated to the ground, leading to N impact points from which the first impact covariance matrix is computed. For lift, the second impact covariance is defined by treating the separation of the two impact points (lift and no-lift) as standard deviations. The third impact covariance matrix, due to wind, is constructed by a more technical procedure that we omit here. The total impact covariance is the sum of the three matrices. The procedure is shown in the flow diagram

$$\Sigma_{EN} = \begin{bmatrix} \sigma^2_E & \rho_{EN}\sigma_E\sigma_N \\ \rho_{EN}\sigma_E\sigma_N & \sigma^2_N \end{bmatrix}$$

in Figure 4.

At the end of the dispersion analysis, each debris group has

$$\Sigma_{EN}\begin{bmatrix} E \\ N \end{bmatrix} = \lambda^2 \begin{bmatrix} E \\ N \end{bmatrix} \Rightarrow \left(\quad _{EN} - \lambda^2 \right) \begin{bmatrix} E \\ N \end{bmatrix} = 0$$

$$\det \begin{bmatrix} \sigma^2_E - \lambda^2 & \sigma_{EN} \\ \sigma_{EN} & \sigma^2_N - \lambda^2 \end{bmatrix} = 0$$

a mean impact point and a covariance matrix defining the impact uncertainties. The covariance matrix (in East-North coordinates) contains the information for finding the size and orientation of the impact ellipse.
The eigenvalues and eigenvectors of Σ_{EN} provide the magnitudes of the major and minor axes and the orientation of the axes.

$$\tan\alpha = \frac{\sigma_N{}^2 - \sigma_E{}^2}{\rho_{EN}\sigma_E - \sigma_N}$$

The two values for λ, solved from the above determinant, are the equivalent values of the standard deviation along the two orthogonal axes rotated by the angle α as shown below. The angle α is determined by the ratios of E/N computed in the above matrix equation after the computed values of λ^2 have been substituted into the equation.

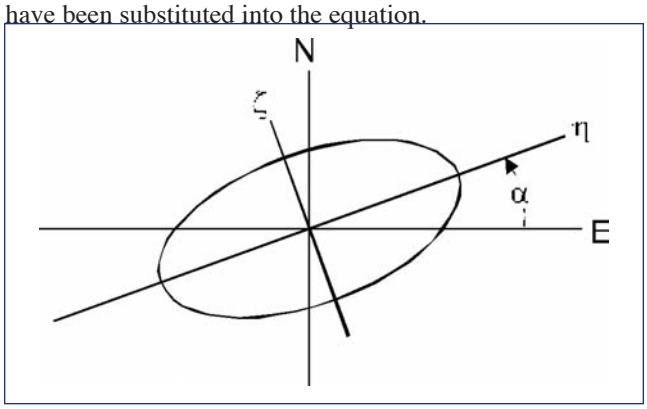

Figure 3. Rotation to a coordinate system withno off-diagonal terms in the covariance matrix.

Figure 4 (facing page). Computation procedure used by CRTF.

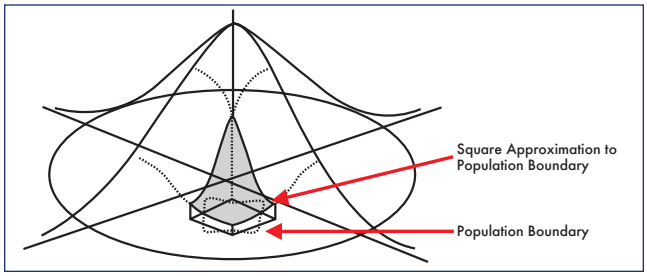

Figure 5. Determination of the equi-density contours.

The ellipse showing the rotation and the relative lengths of the major and minor axes is shown in Figure 3. The two standard deviations ($\sigma_\eta = \lambda_1$ and $\sigma_\xi = \lambda_2$) define a bivariate

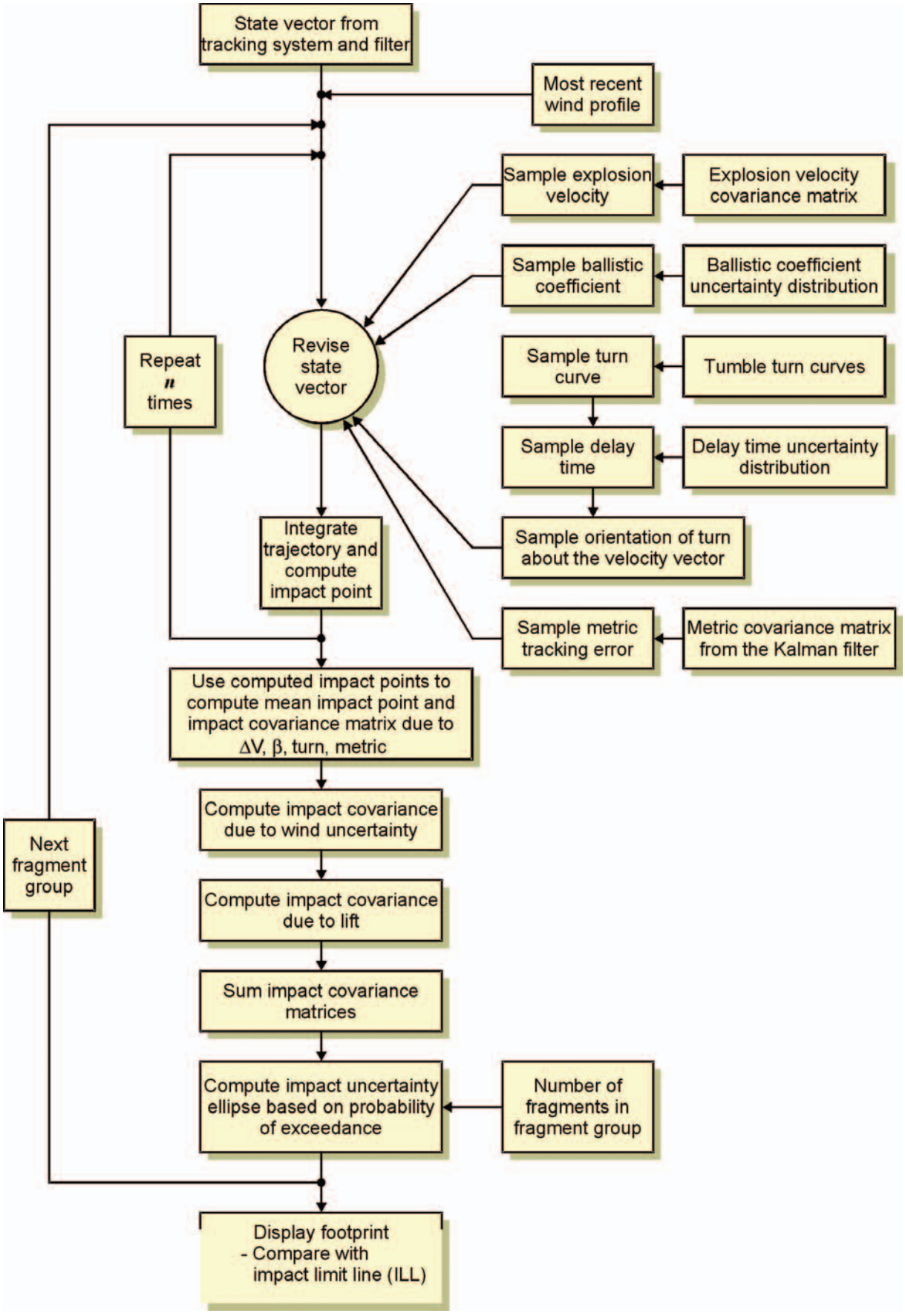
State vector from tracking system and filter
Most recent wind profile
Sample explosion velocity
Explosion velocity covariance matrix
Sample ballistic coefficient
Ballistic coefficient uncertainty distribution
Repeat n times
Revise state vector
Sample turn curve
Tumble turn curves
Sample delay time
Delay time uncertainty distribution
Integrate trajectory and compute impact point
Sample orientation of turn about the velocity vector
Sample metric tracking error
Metric covariance matrix from the Kalman filter
Use computed impact points to compute mean impact point and impact covariance matrix due to ΔV, β, turn, metric
Compute impact covariance due to wind uncertainty
Next fragment group
Compute impact covariance due to lift
Sum impact covariance matrices
Compute impact uncertainty ellipse based on probability of exceedance
Number of fragments in fragment group
Display footprint
- Compare with impact limit line (ILL)

normal distribution that is used to develop isopleths (equi-density contours) of constant impact probability as shown in Figure 5.

The bivariate distribution is also the distribution used to compute impact probability on population centers if the program is to be used for risk analysis.
One option of the program is to surround all of the impact dispersion ellipses with a convex "hull" and use only the hull for display in real-time. A geometrical hull is a curve that bounds a compact set of points.

To give the ellipses and hull a statistical meaning when they reach an impact limit line (ILL), a confidence level C is specified by the user. The ellipses and hull are then resized based on the value of C and on the number of fragments in the group, which in some cases may be in the thousands. The interpretation of the ellipse drawn is that there is a probability C that no fragment from the corresponding fragment group crosses the boundary of the ellipse (such as the ILL). For the hull, C is the probability that no fragment from any fragment group crosses the ILL. The formulas for C for the two cases of debris falling outside of the ellipses and for the debris crossing the tangent to the ellipse (the ILL) are shown below.

The two standard deviations along the major and minor axes are multiplied by a factor z to establish the ellipse size that corresponds to the appropriate probability statement. For "C" probability that no fragment out of N fragments falls

$$z = t - \frac{c_0 + c_1 t + c_2 t^2}{1 + d_1 t + d_2 t^2 + d_3 t^3},$$

outside the ellipse, the formula for z is

$$z = \sqrt{(-2\ln(1 - C^{1/N}))}$$

For "C" probability that no fragment out of N fragments falls beyond a line tangent to the ellipse (such as an ILL), the formula for z is
where $t = \sqrt{(-2\ln(1 - C^{1/N}))}$ and $c_0 = 2.515517$, $c_1 = 0.802853$, $c_2 = 0.010328$, $d_1 = 1.432788$, $d_2 = 0.189269$, $d_3 = 0.001308$.

An additional feature had to be added for explosive debris. When the fragments contain solid propellants that explode on impact, the ellipse radii and the hull are increased by the blast radius corresponding to an overpressure threshold value specified by the user.

The characteristics of some of the debris in free fall may change as a function of time. Solid propellant fragments that burn during descent see a change in both ballistic coefficient and weight. If the propellant fragment completely burns up before impact, this piece will not be included in the impact dispersion set. This results in a reduction in size of the displayed ellipse, or its complete elimination if all the fragments in the group are exhausted. If vehicle breakup occurs in thin or no atmosphere, the solid propellants will be assumed to snuff out before their descent begins.

Figures 6 and 7 show debris footprints for the Space Shuttle and the Titan IV launched from Kennedy Space Center and Vandenberg Air Force Criteria. The ellipses are based on a 95% probability that no fragment will cross any line tangent to any ellipse.

Conclusion

CRTF should provide a valuable tool for range safety at both the Eastern and Western Ranges. It provides an alternate criterion to the traditional vacuum IIP crossing a predetermined abort line as the basis for an abort decision. This approach has been in place for the Space Shuttle for a number of years. CRTF will eventually replace the footprint that is currently in place.

The impact distributions used by CRTF to determine the contours, are the same distributions needed to determine impact probabilities and risks (casualty expectations). Consequently, all of the necessary models to compute risk have also been incorporated into CRTF. One of the program's risk capabilities is to compute contours of constant risk (e.g. 1×10^{-6} conditional probability of casualty) in real time.

Acknowledgement

The authors are particularly grateful for the guidance and support provided by Martin Kinna at the U. S. Air Force Space Command 30th Space Wing and the late Ronald Stout at the 45th Space Wing.

Distribution Statement: Approved for public release, distribution unlimited.

This work was sponsored by the US Air Force Space Command 30th Space Wing at Vandenberg Air Force Base and 45th Space Wing at Patrick Air Force Base under contract number FO4703-91-C-0112.

Footnotes

[1] The numbers given here for casualty probability are somewhat higher than the 0.09 to 0.24 quoted in Section 10.1, Page 21-3 of the CAIB Report, Vol. 1. This is due to an improvement in the probability model made after publication of Vol. 1.
[2] The discrete nature of the model rules out the use of conventional

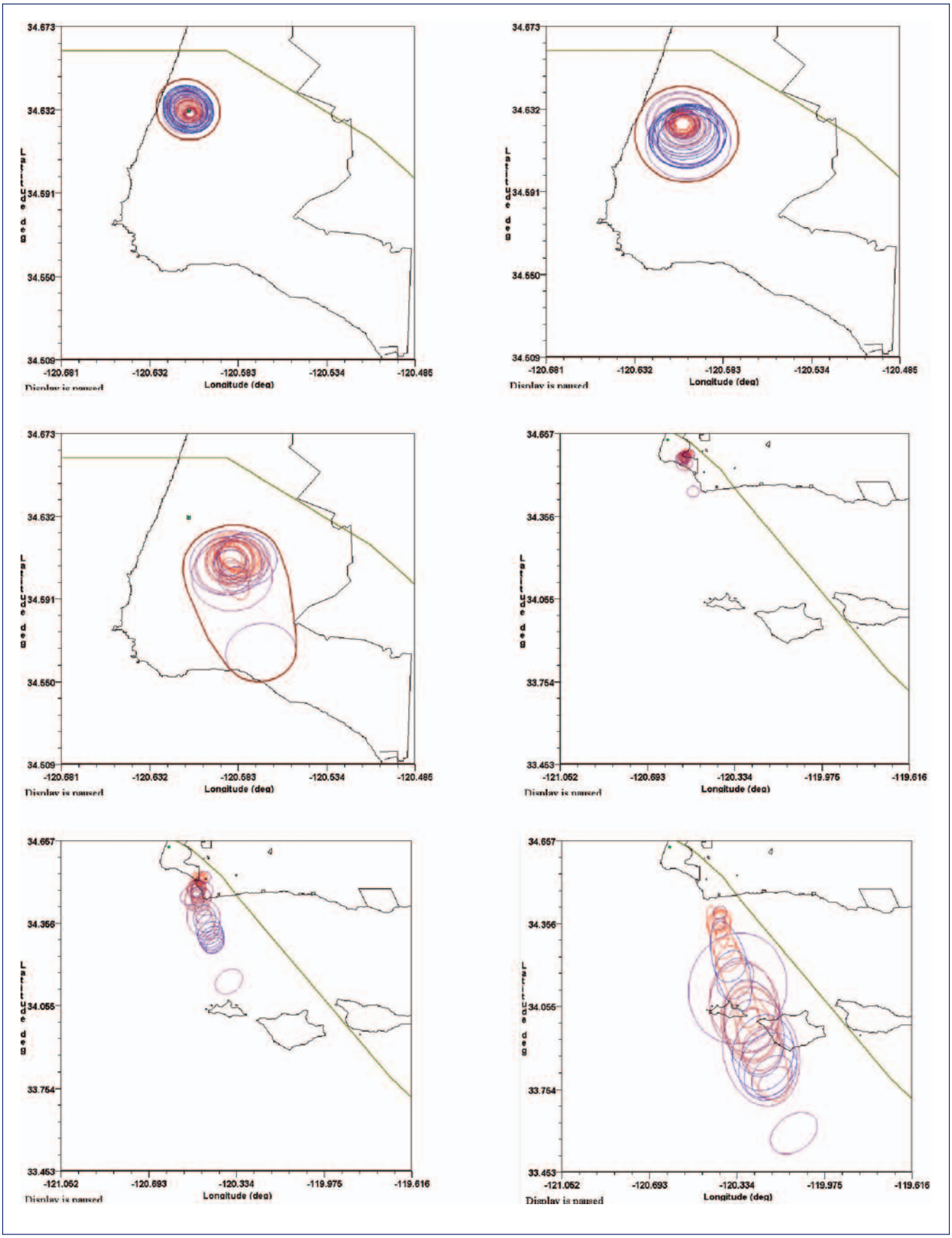

Figure 6. Titan IV Debris Footprints at 15, 30, 45, 60, 75 and 90 seconds after lift-off from Vandenberg Air Force Base (with hull before 60 seconds)).

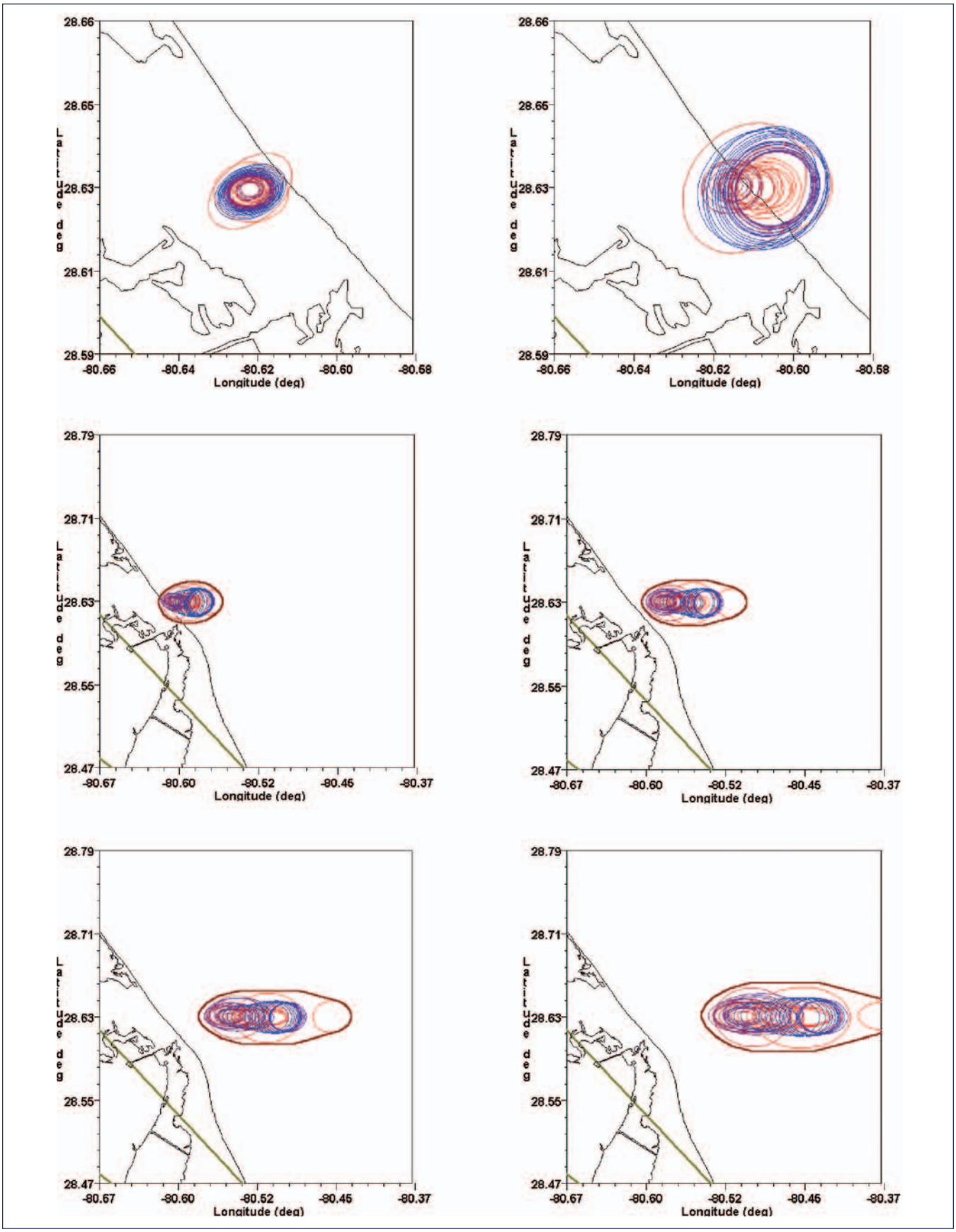

Figure 7. Space Shuttle Debris Footprints at 10, 20, 30, 40, 50 and 60 seconds after lift-off from Kennedy Space Center (with hull after 20 seconds)).